“The Life Cycle of Upper-Level Troughs and Ridges: A Novel Detection Method, Climatologies and LagrangianCharacteristics”

Reply to review #1

We appreciate the positive comments from the Reviewer and also the critical and detailed comments made, which have led to an improved manuscript. In response to the comments made by you and the other Reviewers, we have made considerable changes to the text and figures, and we will mention the relevant ones in our point-by-point response. We uploaded also a special difference PDF, which documents all changes.

Reviewer: My biggest concern is with the authors’ choice of 500 hPa geopotential height (Z500) as the variable for analysis of so called "upper-level" troughs and ridges. As far as I can see, no justification is provided for the choice of this variable. Historically Z500 was widely used in the 1970s and 1980s for analyses of troughs and ridges. However, since PV thinking became mature (cumulating in the seminar paper by Hoskins et al. 1985), synoptic dynamicists have generally accepted that troughs and ridges are manifestation of PV anomalies that have largest amplitudes either at the tropopause or at the surface, and in recent decades, most analyses have focused on analyzing variables either near tropopause level or near the surface (e.g. Hoskins and Hodges 2002, Fig. 1). In this paper, the authors pick the mid-level (500 hPa) for analyses of upper level troughs. Can the authors please provide justification why they pick a mid-troposphere variable instead of an upper troposphere varable to analyze?

Authors: The 500 hPa geopotential height (Z500) has traditionally been used for analysis of troughs and ridges. It is still used amongst forecasters and researchers when describing the synoptic-scale weather evolution in terms of high- and low-pressure systems, and troughs and ridges. Because of its historical significance in synoptic meteorology, we have chosen Z500 in this study for demonstration purposes. Depending on the specific research question, researchers may choose other suitable variables or levels as input data. For example, potential vorticity (PV) or potential temperature on the dynamical tropopause. The use of Z500 in our manuscript is not a statement on its superiority over other variables. The equation used for the computation of the quasi-geostrophic omega forcing however, which is shown in several figures throughout the manuscript, relies on the geopotential height. The combination of the quasi-geostrophic forcing of vertical motion and the geopotential-based troughs and ridges yields a powerful research tool in addition to its use in descriptive synoptic meteorology.

- We supplement the revised manuscript with the results for Z300 (as supplementary figures) and comment briefly on changes between Z500 and Z300 where appropriate.
- We further added a statement that clarifies the use of Z500 for demonstration purposes and that the user of our tool is free to choose other suitable variable or levels depending on the exact research question.

Reviewer: Also, why use curvature of geopotential height contours? Why not use relative vorticity or PV instead? Given that dynamically, we can easily write equations for vorticity or PV tendency while it is difficult to write an equation governing the tendency of curvature of Z500 contours, what are the advantages for picking such a variable to analyze? Can't trough/ridge axes be defined based on vorticity or PV?

Authors: Our approach is to identify troughs and ridges using geometric means in an effort to mimic the human eye. Geometric means have successfully been used to identify streamers (e.g., Wernli and Sprenger 2007), Rossby wave breaking (e.g., Barnes and Hartmann 2012, and many others), Rossby wave initiation (Röthlisberger et al. 2015) and also surface cyclones and anticyclones (closed SLP contours are used in many routines; Neu et al. 2013). Potential vorticity and its curvature could also be used as input data and the user of our tool is free to choose PV instead of Z. In general, vorticity could also be used, but given its rather uneven and noisy distribution over neighboring regions it comes with its own difficulties. In high-resolution NWP data, in particular, the many small-scale relative vorticity maxima become a hindrance in unambiguously identifying troughs and ridges. This is somewhat similar to the challenges of identifying cyclones in high-resolution data based on relative vorticity.

Reviewer: A potential issue is that results can be affected by high terrain, e.g. the Tibetan Plateau. Previous studies (e.g. Chang and Yu 1999, Hoskins and Hodges 2002 (HH02 hereafter); Hakim 2003) have shown that there are upper level waves that propagate along the subtropical jet in winter near the southern edge of the Tibetan Plateau. These waves are clearly missing from this study (Fig. 3a and 4a). These waves are potentially important in understanding Pacific cyclongenesis (e.g. Chang 2005) and the mid-winter suppression (Nakamura and Sampe 2002).

Authors:

(i) The 500-hPa indeed intersects the Tibetan Plateau and other high mountain ranges such as the Rocky Mountains and the Andes. Caution must therefore be given when interpreting the results over these regions. Troughs and ridges are therefore not computed at times and places where missing data values are present in the data.

(ii) It is correct that the North Pacific storm track is fed by two upper-level seeding branches, one coming from the Siberian storm track and another one along the subtropical jet (HH02, Chang 2005). However, it is the northern seeding branch that dominates surface cyclogenesis between Nov–Mar (Hakim 2003, Chang 2005 see discussion on p. 2004/05). The waves along the southern branch are best seen in bandpass-filtered data at 300-hPa along 25° S, typically in composites preceding cases of rather deep cyclogenesis (Chang 2005). Sometimes both seeding branches even interact (Fig. 4 in Chang 2005). In the seasonal mean climatology, we do not see these waves at the 500-hPa level. Most likely the key difference is the time filtering, which excludes waves that act on time scales longer than the typically synoptic times. Thereby these climatologies emphasize a subcategory of

eddies, which otherwise are masked in unfiltered climatologies. This subcategory of waves however is still part of our data, as is shown below for a trough-ridge train along the southern seeding branch between 60–90° E and near 120° E on 26th January 2017. The downstream trough and ridge even connect the northern with the southern seeding branch, which is in agreement with Fig.4 in Chang (2005). In the revised manuscript, we placed a comment on this in the corresponding section.

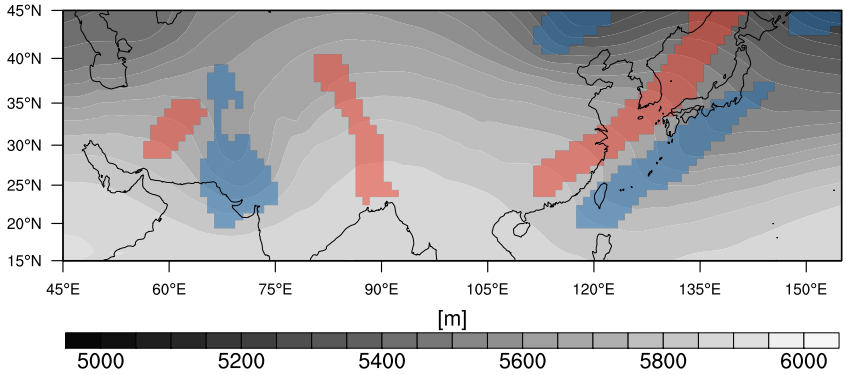

Figure 1: Troughs (blue) and ridges (red) along the southern seeding branch on 26th January 2017.

Reviewer: While the authors discussed some consistencies with previous studies for summer climatology (section 3.2), for the much more researched winter, they didn't provide much comparisons with previous studies. More reference to previous studies should be made in section 3.1. There are some differences that could potentially be due to differences in methodologies. For example, comparing their Fig. 3a to Fig. 11d of HH02, it is apparent that the authors' results are quite a bit further north than those presented in HH02. Also, the authors' results (Fig. 4a) show nearly absence of ridges to the south of Japan, while HH02 shows that 250 hPa Z positive tracks have a maximum south of Japan over western Pacific. Can the authors please explain what might be the reason(s) behind such differences? In any case, comparisons with results from previous studies should be discussed more.

Authors: Thank you for pointing us towards this imbalance between the discussions of the summer and winter climatologies. In the revised version, we now make more comparisons with previous studies, in particular with climatologies of cyclone frequencies and streamers. We do not expect Z500-based troughs and ridges to yield similar climatologies as for bandpass filtered 250-hPa Z eddies (HH02), see our discussion of the southern seeding branch over the Pacific above.

The more poleward location of our climatology (Z500) compared to Fig.11d in HH02, which is based on bandpass-filtered 850-hPa meridional wind, relates to the general westward and poleward tilt with height of baroclinic waves and the relative location of the 500-hPa trough to the surface warm sector.

Note that there is a good agreement between the genesis and lysis hotspots found by HH02 (Fig.5c, d) with the trough and ridge frequencies in our climatologies.

Reviewer: In my opinion, the methodology is not described in sufficient details. How the tracking was done was not really presented and readers are referred to a Ph.D. dissertation (221 pages long). This seems to me an important step since one of the parameters the authors emphasized is age of the system which depends critically on the tracking algorithm. Details of how tracking is done should be presented - perhaps as an appendix or supplemetal material.

Authors: In the revised version, we added a full new and detailed paragraph on the feature tracking in the method section. We also point the reader towards specific pages in the Ph.D. thesis were necessary.

Reviewer: As the authors mentioned, there are always rather arbitrary cutoff values in any objective algorithms. For this algorithm, they mentioned three - the minimum curvature, the size of the trough/ridge objects, and the length of the axis. How sensitive are the results of these choices? How are these choices set? For example, in the example shown in Fig. 2, the trough over the Mediterranean in panel 2a looks to me a very legitimate trough, but it was not identified. I would guess that even 6 hours earlier that trough was already apparent. So, the question is: what is the justification for the authors to pick those particular cutoff values? This is important for genesis and lysis, and for trough ages and lifetimes. In my opinion, sensitivity to these cutoff parameters should be explored and discussed.

Authors: There is unlikely an ultimate answer to this question. Even trained experts will not agree in every situation on the presence of a specific flow feature, which is a lesson learned from the discussion surrounding the detection of fronts (e.g., Schemm et al. 2018), but we do agree that it is important that the cutoff values are discussed. In general, the patterns seen in the winter and summer climatologies (Figs. 3 and 4) are robust. Reducing/increasing the thresholds will emphasize or de-emphasize the centers of action, i.e., detection frequencies will increase or decrease, but they will not change locations. Note also that the thresholds might easily be adjusted for individual case studies to obtain an optimal match to a subjective analysis. This, however, is far more challenging if a climatology of troughs and ridges is compiled. On the other hand, the amplitudes in a climatology might be sensitive to the chosen thresholds to some degree, but we expect the general pattern to be rather robust.

The example in Fig. 2 was *not* used for the tuning of the cutoff values in the algorithm. It was chosen intentionally because we want to present with maximum transparency the difficulties arising from the need to define these cutoff values. This transparency would be missing if we would present a “perfect” case that was used for the tuning (in fact we used, among others, the cases shown in Bue and Xie (2015)). If we reduced the cutoff values to catch the trough already 6 hours earlier, we could almost certainly identify another situation where we would tend to increase the cutoff value again. We believe that it is important that the cutoff values are openly communicated and they are discussed in the method section and also in the illustrative case example.

- Bueh, C. and Z. Xie, 2015: An Objective Technique for Detecting Large-Scale Tilted Ridges and Troughs and Its Application to an East Asian Cold Event. Mon. Wea. Rev., 143, 4765–4783, https://doi.org/10.1175/MWR-D-14-00238.1
- Schemm, S., M. Sprenger, and H. Wernli, 2018: When during Their Life Cycle Are Extratropical Cyclones Attended by Fronts?. Bull. Amer. Meteor. Soc., 99, 149–165, https://doi.org/10.1175/BAMS-D-16-0261.1

Reviewer: Many objective tracking algorithms (e.g. HH02) employ other cutoff values, like feature lifetime and distance travelled. As far as I can see no such cutoffs are employed here. Could the statistics be heavily contaminated by very transient short-lived features like heat lows, or quasi-stationary climatological features?

Authors: We believe that it is natural for quasi-stationary features to dominate the climatology and we regard their presence not as a contamination. They are legitimate members of the trough and ridge family. The transient troughs and ridges are also contained in our data. If necessary, to address a specific research question, the stationary features can easily be removed from the data in a post-processing step or bandpass filtered input data could be used.

Heat lows are excluded. These features are associated with closed contours at the 500-hPa level and are removed from the data. Additional cutoff values like lifetime and distance travelled, which are invoked by some cyclone tracking schemes, are legitimate and can be useful, but they will introduce new degrees of freedom resulting in the same need for a justification as discussed above (How far travelled? How long-lived?). In fact, to obtain the frequencies for troughs with an age between 0-24 hours (Figs. 3 and 4), the trough objects are filtered according to their lifetime.

- The revised manuscript contains a supplement with the trough and ridge climatologies but with short-lived objects removed (a minimum lifetime of 24 hours is required) – see Fig. S3

Reviewer: Some of the statistics shown are not clearly defined. For example, what does trough detection frequency mean? Is that defined based on trough axis or trough objects? Also, what does the "selected frequencies of troughs with an age between 0 and 24 hours (yellow)" in the figure caption of Fig. 3 mean? Without clear definitions of these parameters it is difficult for readers to interpret these figures. Mathematical definition should be provided.

Authors: Thank you for pointing this out.

(i) Detection frequencies are based on the 2d objects. Grid points outside every coherent 2d object are flagged with zeros, grid points insides with ones. Time-averaging over the obtained binary fields yields detection frequencies, which indicate the fraction of time steps affected by a trough or ridge relative to all time steps. We now provide this information in the method section.

(ii) The single yellow contour denotes the frequency that is half the maximum detection frequency for troughs with an age between 0 and 24 hours. To this end, we remove

all 2d trough and ridge objects that are older than one day and re-compute the detection frequency based on the remaining troughs. The yellow contour is half the value of the maximum detection frequency of the thereby filtered troughs.

Reviewer: For the trough age, it is surprising to see that eastern Pacific/Gulf of Alaska is apparently a region where there is high frequency of 0-24-hour troughs (Fig. 3a). I would imagine only regions where there is frequent trough genesis would be highlighted, and that is certainly not a region that is associated with frequent trough genesis. As far as I can see the authors did not mention that region. Can the authors please discuss that?

Authors: The Gulf of Alaska is in agreement with climatologies of streamers (Fig.3 in Wernli and Sprenger 2007) and cycloysis (Fig.5d in Hoskins and Hodges 2002). These references are now mentioned in Section 3.1. Our interpretation is that trough genesis in the Bay of Alaska is resulting from wave breaking and consecutive downstream development during the decaying phase of mature extratropical cyclones over the central Pacific. In this sense, the Bay of Alaska shares some similarities to the trough genesis region over the UK, which, in our opinion, is also a follow-up development driven by upstream decaying mature extratropical cyclones over the eastern North Atlantic.

Reviewer: Apart from the Gulf of Alaska, it seems that "young" troughs and ridges are most frequent over regions with high trough and ridge frequencies (Fig. 3 and 4). Those regions are expected to be regions where troughs and ridges are quasi-stationary and hence presumably "old" rather than "young". Nevertheless, it depends on what the yellow contour really shows as it is not really defined, but this point should be further discussed.

Authors: This is a good point. Downstream of mountains troughs are frequent and thus quasi-stationary, but downstream of mountains troughs are also generated due the flow across the mountain ridge. We believe it is not too surprising that downstream of mountains a trough genesis region is identified. Locally, both the genesis and lysis frequencies are large and troughs growth and decay depend on the flow across the mountains, but they remain stationary at the same time.

Reviewer: In the Lagrangian analysis, one of the authors' goals is to quantify the diabatic impact (p. 14, line 8). My question is whether 500 hPa level is the best level to do that? It is still within the cloud layer at a location where strong heating is still going on. Wouldn't the full impact of diabatic heating be clearer at the tropopause level?

Authors: A comparison between the results based on 500-hPa and 300-hPa troughs and ridges would indeed be insightful. We agree that the full diabatic impact integrated across the entire depth of the troposphere will be more complete if the parcel trajectories were released at a higher level. However, we expect to catch a major part of the condensation, which peaks typically between 850–700 hPa, and also the below-cloud evaporation. Indeed, the trajectories will to a much lesser extent experience diabatic modification due to, for example, freezing. However, if consideration is given to diabatic modification of 500-hPa trough and ridges, it seems natural to release the parcel trajectories from this level.

Overall, this section gives a unique look into a potentially powerful combination of two tools (troughs & ridges plus parcel trajectories), which opens new possibilities for exciting research, but this proof-of-concept is far from being compete. An in-depth analysis would also require several years of trough, ridge and trajectory data and a comparison between trajectories of different lengths and released from different levels or at different trough ages. This would be a study of high scientific merit, in particular if diabatic tendencies from different microphysical processes were available, but a full-fledged stand-alone study on its own would be needed.

Other Concerns:

Reviewer: i) p. 4, line 21: 20S-70N: The authors discussed that they focus on mid-latitude troughs/ridges, but apparently did the analysis in the tropics also. In the tropics, wouldn't the fields be very noisy given the weak geopotential gradient? Why is it necessary to perform the analysis down to 20S?

Authors: The frequency of trough detection drops to zero between 20–25S, the tropics are therefore climatologically not relevant. However, sometimes streamers might elongate far equatorward and we think it is useful to catch those cases as well.

Reviewer: ii) p. 6, lines 4-5: I'm not sure I understand what the authors meant by the sentence "Interestingly here it is a trough over the North Atlantic and the ridge downstream al- ready exists for a longer time period than the up- and downstream troughs". Which troughs and ridges are they referring to in these descriptions?

Authors: We removed the first part of the sentence, it now reads "Interestingly, the ridge downstream already exists for a longer time period than the up- and downstream trough". The synoptic situation appears to be a downstream-development scenario; however, we would expect the upstream trough to be the oldest feature followed by the downstream ridge followed by the next downstream trough. The ridge however is the oldest features, which we did not expect.

Reviewer: iii) While the trough/ridge tilt is indeed closely related to the E-vectors, fundamentally tilted troughs/ridges are related to eddy momentum fluxes (which make up the E-vectors) and have been discussed as early as Jeffries (1926) and Starr (1948).

Authors: The fact that the tilt orientation and the corresponding orientation of the E-vector are fundamentally a result of the eddy momentum flux is mentioned several times throughout the manuscript. In the revised version, we now also define the E vector, and point the reader to the two original papers by Jeffries (1926) and Starr (1948). Thank you for mentioning these two seminal studies.

Reviewer: iv) p.8 line 25: Here the authors write that there is a second maximum near Lake Baikal, which to me is not really accurate since Lake Baikal apparently is located between two relative maxima, one west of 90E and he other over eastern Siberia, northeastern China.

Authors: Yes, corrected and changed to “west of 90E”.

Reviewer: v) Fig. 5: Are the anomalies shown statistically significant? Some of the anomalies seem rather small.

Authors: The anomalies are in good agreement with the anomalies seen in E vectors (Drouard et al. 2015) and we therefore consider them physically meaningful and a good indicator for a consistent change in the orientation during ENSO. The idea here is to compare the results of the two diagnostics against each other and not to show that ENSO produces statistically significant eddy anomaly fluxes. We now set regions where the trough and ridge frequency are below 2% to missing data value.

Reviewer: vi) p. 10, lines 22-23, "more systems will nnow grow on the poleward flank of the jet" this should be quantified or reference cited. Both the jet and storm track shifts equatorward during mid-winter so it is not entirely clear that more systems grow on the poleward flank of the jet. Perhaps a histogram showing the frequency as a functio of tilt would quantify this.

and vii) p. 10, lines 25-26: Same comment as above.

Authors: Please find below a figure for the meridional wind shear of the zonal wind (dU/dy) over the Pacific. During midwinter (black contour), wider parts of the main growth and propagation sector of extratropical cyclones (30-60N) are affected by stronger cyclonic shear, which led us to the interpretation that all poleward tracking storms develop more consistently on the poleward flank of the subtropical jet, assuming that genesis is at a relatively fixed location over the Kuroshio. In agreement with the enhanced cyclonic shear over the Pacific (see below) are the more cyclonically oriented troughs and ridges during midwinter.

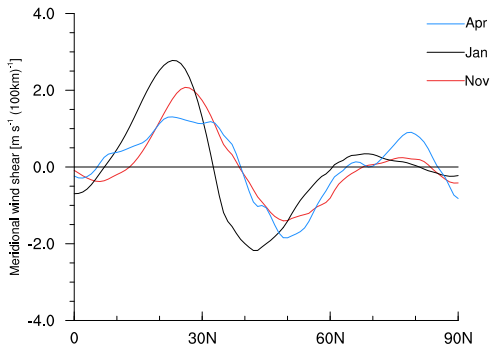

Figure 2: Meridional wind shear of the zonal wind over the Pacific in winter.

Reviewer: viii) p. 10, lines 31-32: "there is no marked reduction in the number of troughs and ridges" This is surprising given the strong decrease in number of troughs found in

Penny et al. Can the authors show the results and provide some explanation on why there is such disagreement between their results and those of previous results?

Authors: This result is an agreement with Schemm and Schneider (2018) who note that the number of surface cyclones in the central Pacific is not decreasing during midwinter. Penny et al. (2010) analyzed upper-level eddy activity at the 300-hPa level in spatially and temporally filtered geopotential height. As is the case with many measures, the midwinter suppression is seen in bandpass-filtered data (eddies and related eddy quantities) but not in measures of the mean flow (mean baroclinicity, mean zonal wind at 300 hPa). It seems as if features identified in raw data, without any frequency filtering (surface cyclones in SLP, Z500 troughs and ridges), exhibit no well-marked suppression, while frequency-filtered measures do. We cannot guarantee that this is the answer, but it appears to be the main methodological difference. In the revised version we added the detection frequencies into the corresponding panels as yellow contours. We find a new localized detection maximum over the eastern North Pacific, which potentially relates to wave breaking and lysis, since detection maximum show a good agreement with cyclolysis frequencies (Fig.5 in HH02). This underpins the presented hypothesis of accelerated, or interrupted, life cycles during midwinter over the eastern North Pacific.

Reviewer: ix) p. 11, line 6: "a fast and intense deepening phase followed by a rapid decay". The familiar LC2 lifecycle of Thorncroft et al (1993) shows a cyclonic lifecycle that decays very slowly. Perhaps the authors should provide references that show rapid decay of cyclonic lifecycles.

Authors: Yes, it is in fact the LC1 that shows an EKE peak followed by a rapid decay (Fig. 4 in Thorncroft et al. 1993). We find however more cyclonically oriented troughs but the reduction in cyclone lifetime was shown in Schemm and Schneider (2018). We thus agree that the familiar and idealized LC2 concept seems not to apply. The LC2 life cycle eventually gets dismantled.

Reviewer: x) p. 12, line 14: Should refer to Fig. 9 here.
Authors: Included.

Reviewer: x) p. 12, line 14: Should refer to Fig. 9 here.
Authors: Corrected.

Reviewer: xi) p. 12, lines 19-20: The windspeed in summer is also weaker so even with the same tilt the vertical motion would still be reduced. This again is related to weaker baroclinicity through the thermal wind relation but still this should be mentioned. Both reduced tilt and reduced wind speed can contribute to decrease in vertical displacement.

Authors: Good point, we added this argument.

.

“The Life Cycle of Upper-Level Troughs and Ridges: A Novel Detection Method, Climatologies and LagrangianCharacteristics”

Reply to review #2

Dear Irina,
Thank you very much for your time and effort you put into this review. We very much appreciate the comments that helped us to improve the paper. Please find below our specific replies. We uploaded also a special difference PDF, which documents all changes.

Reviewer: My major comment has already been picked up by another reviewer: I would also like to see justification of the geopotential level used to identify troughs/ridges and, possibly, how results differ between levels. I can see a point in using an Hgt level as opposed to, e.g., PV, as Hgt levels are readily available in most model outputs, making this approach useful for analysis of, e.g., CMIP6 models. However, troughs/ridges are often seen as upper-level phenomena, while 500 hPa lies in the middle of the troposphere.

Authors: Geopotential height at the 500 hPa level has traditionally been used for analysis of troughs and ridges. It is still widely used for forecasting purposes and also in research. Because of its historical significance, we have used it in this study for demonstration purposes.

In the revised version, we added the results for the 300 hPa level as a supplementary figure and we also comment on notable differences where appropriate. The combination of the quasi-geostrophic forcing of vertical motion by the Q vector, which is formulated using geopotential height, and the geopotential-based troughs and ridges result in a powerful research tool. We see however also the merits of using potential vorticity for input data. The user of our research tool is free to choose any other suitable variable or level as input data depending on the specific research question to be addressed.

Reviewer: Abstract: It is said that tracking allows analysis of evolution of troughs/ridges. However, in my view, this paper does not present such analysis. Either remove this statement from the abstract (it can be kept in the description of the method) or add analysis of their life cycle.

Authors: It is correct, we do not show an explicit example in this manuscript. We changed the sentence in the abstract to “(…) *could be* used to study the temporal evolution of the trough or ridge orientation”. Thanks for pointing this out.

Reviewer: p1, l.21-25: Add a figure showing a trough and a ridge.

Authors: Good idea, we now reference Fig.1.

Reviewer: p2, l.18: define E vector here.

Authors: We added the E vector definition.

Reviewer: p.4, l.9-16: This part needs to be illustrated - draw a figure showing vectors discussed here

Authors: We added such a figure.

Reviewer: p.5, l28: give a brief description of Q vector here first, not only a reference.

Authors: We added a brief description of the Q vector.

Reviewer: p.6, l22: can the absence of troughs be a result of northern boundary at 70N? Could it be that troughs extent further north and the part to the south of 70N is below the threshold on the length?

Authors: Our statement that troughs are absent at the end of the North Atlantic storm track was inaccurate. It is the center over the UK and over eastern Europe that is associated with development at the end of the North Atlantic storm track. We corrected this statement.

Reviewer: p.5, l. 32: The map at 06 UTC also suggests a significant trough in the Mediterranean, but it remains undetected. Is it due to the thresholds? In this case, some sensitivity test should be shown to justify the selection of thresholds.

Authors: The case study was chosen intentionally to highlight the difficulties arising from the need to define thresholds. The presented case was not used for the tuning of the thresholds. There is unlikely an ultimate answer to this question, because when we decrease the threshold in this case, we will find another where we would tend to increase it again. We do not want to show the perfect example in our study. We want to be transparent about this issue. We discuss for this reason the role of the thresholds in the corresponding section. In general, the patterns seen in the climatologies are robust, but the amplitude of detection frequencies depend on the used threshold. This holds true for all object-based feature detection algorithms.

Reviewer: p.6, l. 17: Is it frequency of trough area of trough axes?

Authors: Here we use the trough objects corresponding to the through area. We added this information.

Reviewer: p. 7, l.1: To confirm that Greenland troughs are more transient can you built pdfs of trough lifetime characteristics (propagation speed and lifetime) in regions of interest (over Greenland, Pacific that is discussed later and a reference region).

Authors: The Figure below shows the winter climatology of the trough lifetime at each grid point. The lifetime at Greenland is reduced compared to downstream of the Rocky Mountains or compared to East Europe and Russia. We added the figure as supplement to our manuscript.

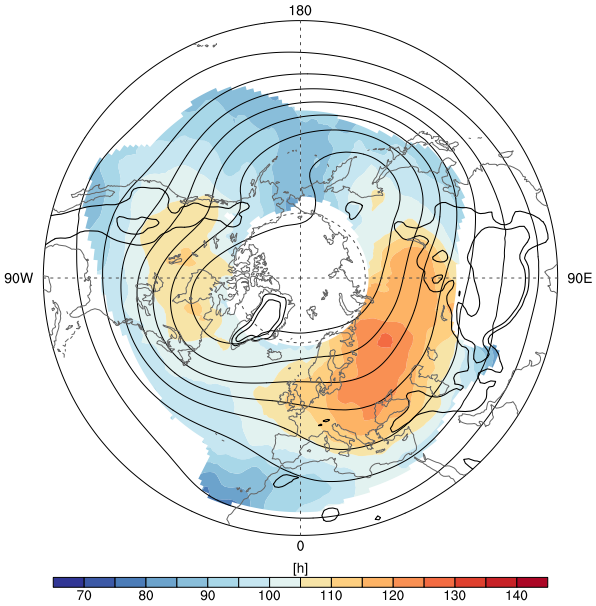

Figure 1: Mean lifetime of troughs during the extended winter period (Nov–Mar).

Reviewer: p7, l28-30: Given the difference in frequency of troughs and ridges, did you think of applying different thresholds for their identification. Troughs and ridges can be seen as advection of cold and warm air and, due to the variable air density, typical curvature of hgt may vary.

Authors: This is a very interesting suggestion, but we do not find a difference in the curvature between through and ridges. Climatologically, the curvature varies between the lower threshold of 0.05 degrees/km to 0.13 degrees/km for troughs and ridges. In midlatitudes both have a mean curvature of 0.1 degrees/km. However, we did some experiments with a latitude dependency of the thresholds, but did not consider this approach further as it is mainly relevant for regions that we have excluded (<20S and >70N) from our data.

Reviewer: p.8: Can you think of reasons why there is no cyclone maximum near the Iberian Peninsula associated with a peak in trough frequency and Rossby wave breaking? I suggest that these conditions in the upper (middle) troposphere produce cut off lows not visible on the surface.

Authors: Yes, we agree. It is likely cut-off low formation that is taking place in this region. We added this information.

Reviewer: p.8, l34: Despite equatorward shift of troughs off the West coast of the US in summer, the ridges shift poleward during summer (something that one would have expected). Can you discuss what may cause summer poleward shift of troughs in this region?

Authors: We assume that PV streamer formation is more common in this region. Consider the schematic below from Thorncroft et al. (1993). If PV streamer formation, or cut off

formation, is more common (upper panel), the more equatorward elongating troughs will result in a more equatorward displaced anomaly.

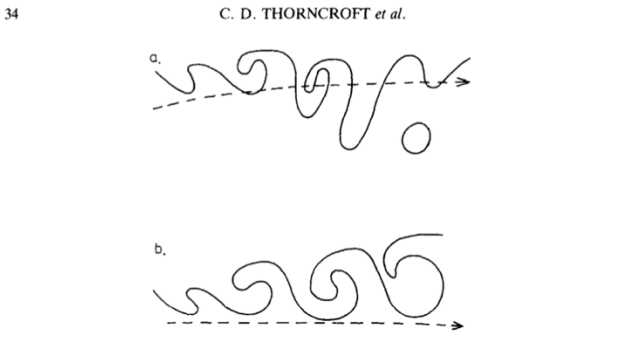

Figure 12. Schematic of a PV-theta contour in an Atlantic storm track sharing its main characteristics with (a) an LC1-type life cycle and (b) an LC2-type life cycle. The dashed line marks the approximate position of the mean jet at each stage.

Reviewer: p.10, l33: The text refers to Fig 6, which shows mean orientation of ridges and troughs. This plot is supposed to illustrate the 'dominance' of those systems in the Pacific, however, I think the frequency should be shown instead.

Authors: Ok, we corrected the sentence since "dominance" is misleading. We want to highlight however the fact that the preferred orientation is now cyclonic over most parts of the Pacific, while this is not the case during the shoulder months. We do not refer to the frequency, but to the preferred orientation regardless of the frequency.

Reviewer: p.11: Did you test longer backward trajectories? Do troughs/ridges have life cycles? It will be nice to see some analysis on this. Are back trajectories in fig. 7 b,c sensitive to the stage of their development?

Authors: We did not test longer backward trajectories, but it is good to see that this section triggers a lot of interesting questions and further suggestions from both reviewers. We consider longer trajectories to be in particular useful for Z300-based troughs and ridges.

We agree that troughs and ridges have a life cycle. However, while we do know their age, it appears to us not as particularly meaningful to release the trajectories from features of similar age. Cyclones, for example, are often categorized according to their genesis, maximum deepening, maximum intensity, maximum decay and lysis. Such a definition can be based on, for example, changes in SLP along each cyclone track. We do not have a similar convention for troughs and ridges. A proper definition of the life cycle stages of troughs and ridges would be required on which the community agrees. This section "only" explores the now new possibility of using the trough and ridge objects as trajectory start location in a "proof-of-concept" fashion. It is not indented to be a complete analysis. We agree that a complete analysis would be very interesting, with different levels and different trajectory lengths, for a complete 30-year period and for different life cycle stages on both hemispheres. All of these questions would easily fill one or two completely new studies and we cannot perform them in this paper.

Reviewer: p.12: A histogram of north/south displacements might be interesting. It is worse noticing that fig. 8a,b and e,f are in good agreement with each other, i.e. decent

corresponds to a reduction in potential temperature. However, then the statement that the downward motions occur along isentropic surfaces sloping equatorward is questionable (though I like to think that the flow is along isentropes).

Authors: We agree, there is on average a mild decrease in potential temperature so the motion is not fully isentropic, but quasi-isentropic. This reduction is found along trajectories that exhibit also a weak downward motion of 0-100hPa in 24 hours starting from the 500 hPa level and we therefore speculate that this is due to radiative cooling. We corrected this statement in the revised manuscript.

Reviewer: p.12, l2: what is the difference between a trough with closed geopotential isolines and a cyclone at that level?

Authors: Yes, it could be a deep surface cyclone or cut-off low with no surface signature, but we want to treat those distinct from "pure" troughs and ridges and the algorithm thus labels the former as closed-contour or closed troughs and the latter and open troughs. Although the distinction between closed and non-closed (open) troughs is somewhat arbitrary, it also matches with a human forecaster's perspective. And, as stated in the manuscript, it is also partly the aim of our approach to mimic the geometric view of a human forecaster.

Reviewer: p14, l.10: Is the code available online?

Authors: We are happy to share the data and the code. As is the case for all our feature-based climatologies, the data will be provided at http://eraiclim.ethz.ch (see Sprenger et al. 2017 for a full list of available climatologies; note that we are in the transition to ERA5 data) and the Fortran and Python codes will be made available on request.

- Sprenger, M., et al. 2017: Global Climatologies of Eulerian and Lagrangian Flow Features based on ERA-Interim. Bull. Amer. Meteor. Soc., 98, 1739–1748, https://doi.org/10.1175/BAMS-D-15-00299.1

Reviewer: Abstract: "methods that detect the initiation phase of upper-level Rossby wave development" - did you mean Rothlisberger et al. 2016 paper or another? I could not find a paper on this in the references.

Authors: Yes, this was missing, we added a reference to the introduction.

Reviewer: p1, l.22: for a good reason.

Authors: Corrected.

Reviewer: p1, l.24: replace enchanted with increased.

Authors: Corrected.

Reviewer: p2, l.3: re-phrase to read better.

Authors: We tried to simplify the sentence.

Reviewer: P6, l19: change to 'Altai' (multiple times in the paper). Not sure whether this is still east Asia. Perhaps, Far East is better.

Authors: We changed the wording consistently to "Altai". Maybe Far East is a bit ancient. We removed East Asia as suggest and no consistently refer to Altai (the latter is partly in East and Central Asia).

Reviewer: P.6, l20: remove 'slightly'

Authors: Removed.

Reviewer: Fig. 3, 4: On my screen continents are barely visible. As for elevated areas, I suggest either marking them with a different colour or hatching.

Authors: We did some experiments with hatching, but turned out to look rather patchy in the printed version. We will make sure, together with the editing team, that during the typesetting the quality of the continents will be increased. We did not use the high-quality figures for the initial submission and will submit higher-quality figures to the editorial office.

Reviewer: p.11, last line: I am not sure why you say 'pushing air', I guess it is being pushed. Perhaps 'moving air' is better.

Authors: Yes, perhaps "moving air" is better, we replaced "pushing air" with "moving air".

Reviewer: p.12, l6: remove 'most'

Authors: Corrected.

Reviewer: p.12, l3: change 'ore' to 'or'

Authors: Corrected.

Thank you for the helpful comments!

“The Life Cycle of Upper-Level Troughs and Ridges: A Novel Detection Method, Climatologies and Lagrangian Characteristics”

Reply to review #3

We would like to thank Reviewer #3 for the specific and positive comments on how we can improve the presented manuscript. In response to the comments made by you and the other Reviewers, we have made considerable changes to the text and figures, and we will mention the relevant ones in our point-by-point response. We uploaded also a special difference PDF, which documents all changes.

Reviewer: As one of the most important skills of this tracking algorithm is finding the axis of the system, and a lot of the analysis is based on it, more effort should be invested in explaining the notation of cyclonic and anticyclonic tilt, what are the factors controlling the axis orientation and the effect of the axis orientation on the life cycle of the system and it’s interaction with lower-level systems. A cartoon demonstrating these concepts might be helpful.

Authors: The ideal schematic to present the notion of cyclonic and anticyclonic tilt is in our opinion Fig. 12 of Thoncroft et al. (1993), which is shown below. We now reference explicitly this schematic in our introduction.

Further, we added a new Figure that explains the algorithm and, in that schematic, we added a trough axis and point the reader to the orientation of this axis to illustrate the notion of cyclonic and anticyclonic orientation (New Figure 2).

34 C. D. THORNCROFT *et al.*

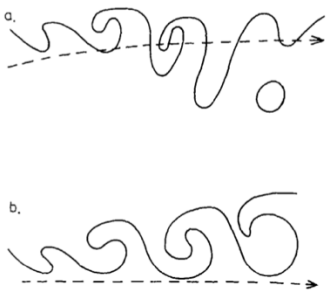

Figure 12. Schematic of a PV-theta contour in an Atlantic storm track sharing its main characteristics with (a) an LC1-type life cycle and (b) an LC2-type life cycle. The dashed line marks the approximate position of the mean jet at each stage.

Reviewer: In the introduction, more attention should be given to explain the open questions addressed in this work (ENSO, midwinter minimum), and how these questions might be addressed using tracking algorithms.

Authors: Good point, we added a new paragraph to the introduction that explains the research questions related to ENSO and the midwinter suppression, which we address in our study. The main literature overview is however presented in the corresponding sections to keep the introduction concise.

Reviewer: Choosing 500 hPa as the main level in which the analysis is done is reasonable, but the authors should add a figure describing the performance of the algorithm as a function of tracking level to give a more general representation.

Authors: Ok, we added the results of the 300 hPa level as a supplement figures and now mention the possibility for the user to choose the level and variable.

Reviewer: The effect of ENSO and the midwinter suppression on the number of eddies is crucial in understanding their overall effect. Although it is challenging to measure as it appears differently depending on the tracking algorithm and the parameter that is tracked. Therefore, the effect of ENSO and the midwinter suppression on the number of tracked eddies as found by the described algorithm should be shown (either in figures 5 and 6 or as additional figures).

Authors: With respect to the influence of ENSO, we focus on the change in the orientation because this was previously inferred based on **E** vectors. We would like to demonstrate the correspondence of the two perspectives. With respect to the midwinter suppression, we fully agree, here the number/frequency of identified objects matters and we added the detection frequencies as yellow contours to the revised Fig. 6.

Reviewer: One of the most commonly used Lagrangian methods is creating composites based on the tracking data. Using this algorithm in order to make composites might be even more useful as the algorithm finds the region associated with the systems, and improved composites can be made. Adding a composite analysis of some field might be very interesting (for example, a composite of the vertical velocity can be made and later compared to the more complicated analysis using LAGRANTO).

Authors: Yes, composites are indeed a major application, which we also foresee for the troughs and ridges. Troughs and ridges could be centered on cyclogenesis or extreme events. We prefer not to add another figure to the paper because the number of Figures is already large. We now have already 10 Figures (1 new, 2 modified) plus 3 new supplementary Figures. We believe that a composite analysis deserves a full-fledged study.

Reviewer: The analysis shown in figure 7 is confusing. These eddies are, to a good approximation, a closed system and therefore mass (and PV) conserving. Looking at the total vertical movement of parcels does not necessarily mean much and the conclusion that vertical processes play a small role in the dynamics might be incorrect. Previous papers (e.g., Booth et al., 2015; Tamarin-Brodsky and Hadas, 2019) have shown (as in figure 8), that there is a small section of rapidly ascending air and a larger section of moderately descending air.

Authors: The trough in Fig.7 is classified as an open trough, because the corresponding geopotential isolines (blue contours in Fig. 7) are not closed. The closed area in Fig. 7 is the region satisfying the curvature threshold (red contours in Fig. 7). We therefore expect a continuous flow in and out of the trough area, which is suggested also by the trajectories. We are not sure in which sense the through constitutes a closed system, for a truly closed

system we would expect the trajectories to circle to some degree inside the closed contour. We however fully agree that analysis of mean quantities can be misleading in particular if the spread among the air parcels is large. Therefore, we added two new histograms to Fig. 7, which show the binned 24-hour changes in PV and pressure. PV changes are for 90% of all air parcels strongly confined to -0.2 to 0.2 PVU/24h. Thus, it is fair to argue that the flow is almost adiabatic with a small fraction of air parcels undergoing diabatic modification (of up to -0.6 PVU/24h). Pressure changes indeed reach up to 60 to 80 hPa/24h for approximately 15% of all air parcels, while ascent of up to -30 to -40 hPa/24h is found for less than 5%. It is therefore correct, as you point out, that embedded in the large-scale descending motion there is a very small fraction of ascending air. Similar examples occur for convection embedded in warm conveyor belts (Martínez-Alvarado et al., 2014; Rasp et al. 2016; Oertel et al. 2019), which itself is the more rapidly ascending fraction of air inside the rising warm sector of an extratropical cyclone. We comment on this in the revised manuscript.

Reviewer: Figure 1 can be reduced to 3 subfigures, combining subfigure b-c and e-f and describe the system's age in the text.

Authors: This is correct. We will check with the copy editor if the figure is too large and reduce it to 3 subfigures but if not, we prefer to keep it.

Reviewer: The use of the phrase "low- (high-) pressure system" (e.g., page 4, line 24) is con- fusing in this context, as it is mostly used to refer to low-level cyclones (anticyclones).

Authors: Yes, this cyclone is also well-marked at the surface. We now mention this in the text, which hopefully clarifies the wording.

Reviewer: The climatology calculations that led to the colours and contours in figure 3 should be better explained.

Authors: We tried to improve the explanation.

Reviewer: Page 11, line 32 to page 12, line 2: These results have been discussed before in the context of extratropical storms, both in simulations (Booth et al., 2015), and observations (Tamarin-Brodsky and Hadas, 2019). A reference should be made.

Authors: Yes, the asymmetry is not an entirely new finding. We added the studies of Sinclair et al. (2020), Tamarin-Brodsky and Hadas (2019), Booth et al. (2015), plus the original literature of O'Gorman (2011), who first explained the asymmetric distribution of vertical motion as a result of the influence of moisture and heating on the static stability. We would argue that the asymmetry is also resulting from moist convection being mostly upward in the atmosphere and not downward.

Reviewer: Page 3, line 17: "The trough and ridge identification algorithm is based on...". Per- haps use "The trough and ridge identification are done on..."

Authors: The corresponding sentence was changed.

Reviewer: Page 4, line 20: Number is unclear.

Authors: The number is the trough/ridge area.

The Life Cycle of Upper-Level Troughs and Ridges: A Novel Detection Method, Climatologies and Lagrangian Characteristics

Sebastian Schemm [1], Stefan Rüdisühli [1], and Michael Sprenger [1]

[1]Institute for Atmospheric and Climate Science, ETH Zurich, Zurich, Switzerland

Correspondence: Sebastian Schemm (sebastian.schemm@env.ethz.ch)

Abstract. A novel method is introduced to identify and track the life cycle of upper-level troughs and ridges. The aim is to close the existing gap between methods that detect the initiation phase of upper-level Rossby wave development, and methods that detect Rossby wave breaking and decaying waves. The presented method quantifies the horizontal trough and ridge orientation and identifies the corresponding trough and ridge axes. ~~The trough and ridge axes~~ These allow us to study the dynamics of pre- and post-trough~~or~~ /ridge regions separately. The ~~tracking allows us to study the temporal evolution of the trough or ridge orientation. The~~ method is based on the curvature of the geopotential height at a given isobaric surface and is computationally efficient. Spatio-temporal tracking allows us to quantify the maturity of troughs and ridges, and could also be used to study the temporal evolution of the trough or ridge orientation. First, the algorithm is introduced in detail, and several illustrative applications ~~,~~ – such as a downstream development from the North Atlantic into the Mediterranean ~~,~~ – and seasonal climatologies are discussed. For example, the climatological trough and ridge orientations reveal strong zonal and meridional asymmetry~~. Over~~ : over land, most troughs and ridges are anticyclonically oriented, while they are cyclonically oriented over the main oceanic storm tracks~~. The~~ ; the cyclonic orientation increases ~~towards~~ toward the poles, while the anticyclonic orientation increases ~~towards~~ toward the equator. Trough detection frequencies are climatologically high downstream of the Rocky Mountains and over East Asia and Eastern Europe, but are remarkably low downstream of Greenland. Furthermore, the detection frequencies of troughs are high at the end of the North Pacific storm track, ~~but no comparable signal is seen over the North Atlantic~~and at the end of the North Atlantic storm track over the British Isles. During El Niño-affected winters, troughs and ridges ~~tilt anomalously strong cyclonically~~ exhibit an anomalously strong cyclonic tilt over North America and the North Atlantic, in agreement with previous findings based on traditional variance-based diagnostics such as **E** vectors. During La Niña the situation is essentially reversed. The orientation of troughs and ridges also depends on the jet position. For example, during midwinter over the Pacific, when the subtropical jet is strongest and located farthest equatorward, cyclonically orientation troughs and ridges dominate the climatology. Finally, the identified troughs and ridges are used as starting points for 24-hour backward parcel trajectories, and a discussion of the distribution of pressure, potential temperature and potential vorticity changes along the ~~flow path~~ trajectories is provided to give insight into the three-dimensional nature of troughs and ridges.

1 Introduction

Troughs and ridges are ubiquitous flow features in the upper troposphere and are centerpieces of weather and climate research, ~~and~~ for good reason. In general, a trough is associated with cyclonic flow and ~~pushing~~ moving cold air equatorward. It is depicted as a region of reduced geopotential height on an isobaric surface, or enhanced potential vorticity on an isentropic surface. The counterpart of a trough is a ridge, which is associated with warm air ~~pushing poleward, enhanced geopotential height~~ ~~(~~moving poleward, increased geopotential height – corresponding to reduced potential vorticity ~~PV)~~ (PV) – and anticyclonic flow. Jointly, a trough and a ridge form the positive and negative phases, respectively, of large-scale Rossby wave patterns, which shape weather development in the mid-latitudes. At the equatorial tip of a trough, where the geopotential isolines are closely aligned~~(or the PV gradient is at a maximum)~~, a jet streak can form, and the conservation of the absolute vorticity and a region of diffluent flow predict forced upward motion in the jet exit region~~predict large-scale upward motion~~. It is therefore not too surprising that surface cyclogenesis (Petterssen and Smebye, 1971; Sanders, 1988; Lackmann et al., 1997; Graf et al., 2017), rapid cyclone intensification (Sanders and Gyakum, 1980; Wash et al., 1988; Uccellini, 1990; Wernli et al., 2002; Gray and Dacre, 2006) and enhanced precipitation (Martius et al., 2006; Massacand et al., 2001; Martius et al., 2013) usually take place in the region ahead of the upper-level trough axis.

The shape and orientation of troughs and ridges is pivotal in determining their influence on synoptic-scale flow evolution. A trough ~~,~~or a ridge ~~,~~tilts cyclonically if it forms under cyclonic shear, while it acquires an anticyclonic orientation if it forms under anticyclonic shear (Davies et al., 1991; Thorncroft et al., 1993). In the case of a pronounced equatorward (poleward) excursion of a trough (ridge), it may wrap up and undergo irreversible deformation in a wave breaking event (McIntyre and Palmer, 1983; Thorncroft et al., 1993). Under anticyclonic shear, the trough deforms into a narrow band, called a streamer, which extends equatorward to the mean jet position. During the associated wave breaking event, the jet is pushed poleward. With cyclonic shear, wave breaking occurs poleward of the mean jet position, thereby pushing the jet equatorward (Thorncroft et al., 1993; Lee and Feldstein, 1996; Orlanski, 2003). The notion of cyclonically and anticyclonically oriented wave development is schematically summarized in Fig. 12 in Thorncroft et al. (1993). This process, through which cyclonically or anticyclonically breaking troughs and ridges displace the jet, is even able to excite positive or negative North Atlantic Oscillation events (Benedict et al., 2004; Franzke et al., 2004; Rivière and Orlanski, 2007). A traditional means for quantifying the influence of upper-level troughs and ridges on the jet strength and location is the **E** vector (Hoskins et al., 1983; Trenberth, 1986). With anticyclonic shear, troughs and ridges acquire an anticyclonic orientation, and the **E** vector points equatorward, indicating poleward eddy momentum flux. With cyclonic shear, a poleward-pointing **E** vector indicates southeast-to-northwest-oriented troughs and ridges, which correspond to a cyclonic orientation, and the corresponding equatorward eddy momentum flux pushes the jet equatorward (Hoskins et al., 1983; Rivière et al., 2003).

Troughs and ridges actively interact with diabatic processes and are far from being dry adiabatic flow features. Ahead of the trough axis, where upward vertical motion prevails, air from the surface warm sector of a cyclone is lifted within the warm conveyor belt (WCB) to upper levels (Harrold, 1973; Browning, 1986, 1990; Wernli, 1997). During ascent, the air is diabatically modified ~~, for example , by condensation ,~~ – for example by condensation – in a way that amplifies the upper-level

ridge and the anticyclonic flow downstream of the surface cyclone (Stoelinga, 1996; Wernli and Davies, 1997; Grams et al., 2011; Schemm et al., 2013). This process also amplifies the streamer formation (Massacand et al., 2001) and accelerates the jet. From a PV perspective, this phenomenon is seen as a negative PV anomaly around the WCB outflow, corresponding to enhanced anticyclonic circulation~~, and by~~. It is also associated with a sharpening of the PV gradient along the edge of the WCB outflow, ~~corresponding to an accelerated~~ which corresponds to an acceleration of the jet. From a momentum flux perspective, the center of the WCB outflow corresponds to a region of enhanced horizontal eddy momentum flux divergence (leading to a deceleration), and the edge of the WCB outflow corresponds to a region of enhanced eddy momentum flux convergence (leading to an acceleration) (Schemm, 2013). The WCB outflow ahead of an upper-level trough has thus been shown to accelerate downstream cyclone growth (Wernli and Davies, 1997; Pomroy and Thorpe, 2000; Grams et al., 2011; Schemm et al., 2013) and can even lead to the formation of large-scale blocks (Pfahl et al., 2015; Steinfeld and Pfahl, 2019). Recent studies have presented further evidence for the non-negligible role of turbulence and radiation in the diabatic modification of the life cycle of troughs and ridges (Spreitzer et al., 2019). The dynamics of troughs and ridges thus may act as a stepping stone ~~towards~~ toward a better understanding of the coupling between adiabatic and diabatic processes and allows for the connection of atmospheric processes from the planetary scale to the mesoscale.

In this study, a novel feature-based method is introduced for identifying and tracking the life cycle of upper-level troughs and ridges, including their axes and orientations, in gridded data. Feature-based methods for detecting streamers (Wernli and Sprenger, 2007), Rossby wave initiation (Röthlisberger et al., 2016), and wave breaking (e.g., Postel and Hitchman, 1999) events are widely used research tools, and the motivation behind this work is to extend the capability of available tools and to track and characterize the entire life cycle of upper-level troughs and ridges from genesis to lysis. We further aim to compare the detected life cycle characteristics of, for example, the trough orientation ~~,~~ with previous results obtained from more traditional methods such as the aforementioned **E** vectors, thereby bridging gaps between different perspectives on synoptic-scale evolution.

The trough and ridge detection is used to derive winter and summer climatologies of their frequency and orientation. Further, we address two research questions discussed in the recent literature. The first concerns the change in the orientation of downstream propagating eddies during winters affected by the El Niño–Southern Oscillation (ENSO): During La Niña, eddies are assumed to acquire a more anticyclonic orientation over North America, while they acquire a more cyclonic orientation during El Niño (Li and Lau, 2012a, b; Drouard et al., 2015). Previous studies used the **E** vector (Hoskins et al., 1983; Trenberth, 1986) to study the eddy orientation. Here, we quantify the trough and ridge tilt using the automated algorithm. The second research question concerns the midwinter suppression of the North Pacific storm track: During midwinter, the potential for cyclone growth is largest, but – in contrast to the North Atlantic – the observed storm track intensity over the Pacific is lower compared to the shoulder seasons (e.g., Nakamura, 1992). Using the trough and ridge detection, we explore potential changes in the orientation of troughs and ridges, because a stronger cyclonic orientation is typically associated with more intense cyclones (e.g., Fig. 4 in Thorncroft et al., 1993). More detailed literature overviews are presented in the corresponding sections. Finally, we explore the possibility to use the trough and ridge objects as starting regions for air parcel trajectories in an effort to explore the diabatic modification of the life cycle of troughs and ridges.

The paper is organized as follows. Details of the algorithm and a case study are presented in Section ~~2, and~~ 2. Section 3 is dedicated to the discussion of winter and summer climatologies ~~,~~ and the change in the trough and ridge orientation during ENSO-affected winters and over the Pacific in midwinter. In Section 4, we explore troughs and ridges from a Lagrangian viewpoint before concluding the paper in Section 5.

2 Data and Methods

The trough and ridge identification algorithm ~~is based on~~ uses 6-hourly ERA-Interim data (Dee et al., 2011) but can easily be applied to other gridded data sets. The reanalysis data are provided publicly by the European Centre for Mid-Range Weather Forecasts (ECMWF) via URL <apps.ecmwf.int/datasets>. More specifically, the identification is ~~based on the 500-hPa~~ demonstrated on the 500 hPa geopotential height data, which are interpolated onto a regular $1^\circ \times 1^\circ$ grid. ~~The~~ Results based on the 300 hPa geopotential height data are shown in a supplement. The 500 hPa geopotential height has traditionally been used for analysis of troughs and ridges and continues to be used for research and forecasting purposes. The presented method is, in general, also applicable to different levels or variables, e.g., 300 hPa geopotential height, isentropic PV or potential temperature on the dynamical tropopause. Depending on the exact research question the most suitable level and variable can be chosen. The investigation period is ~~1979–2018~~1979–2018, and the monthly mean trough and ridge climatologies are publicly available ~~at URL <~~[eraiclim.ethz.ch~~> (Sprenger et al., 2017)~~; Sprenger et al. (2017)].

This section describes in detail how the trough and ridge axes are identified and tracked. Three distinct steps are involved:

- identifying 2D trough and ridge objects (masks) and their corresponding axes;
- tracking the trough and ridge objects and quantifying their age and overall lifetimes;
- characterizing the horizontal orientation of each trough and ridge axis.

The following subsections will address specific aspects of the algorithm, including a detailed validation.

2.1 Trough and Ridge Identification

The identification of troughs and ridges starts with the geopotential height at, for example, 500 hPa, as seen in Fig. 1a for 12 UTC on 12 January 2010. Two distinct troughs and one ridge can visually be identified: a northwest-to-southeast oriented trough over the eastern North Atlantic, which is associated with a mature low pressure system to the west of Ireland; a meridionally oriented ridge, which extends from the Iberian Peninsula to the ~~UK~~British Isles; and a meridionally oriented trough over the Central Mediterranean to the southeast of Italy over the Ionian Sea. The goal of an ~~automated~~ object-based trough and ridge detection is to automatically identify these features and the corresponding axes. Several aspects have to be kept in mind. First, the smooth geopotential isolines shown in Fig. 1a do not reflect the underlying $1^\circ \times 1^\circ$ ERA-Interim grid, but are already smoothed due to the contour drawing algorithm. Therefore, in the following panels (Fig. 1b to f), the geopotential height is shown on the underlying input grid. Second, troughs and ridges may exhibit a complicated structure. For instance, the

horizontal orientation ~~varies~~ can vary along a trough or ridge axis; a trough or ridge can be broken into different segments; and the curvature of the geopotential isolines can considerably vary over small distances. The challenge for an automatic detection algorithm is to identify all these different characteristics. In the following, details of the proposed algorithm are described.

~~Geometrically, we~~ We suggest to identify troughs and ~~ridge~~ ridges geometrically using the curvature of the geopotential isolines. To this end, the change of the orientation of a vector pointing along an isoline is computed. First, at every grid point, the gradient of the geopotential field is calculated and the gradient vector is rotated by 90°, such that the rotated vector aligns with the geopotential isolines. Next, a new location 5 km in the direction of the aligned vector is determined, and the corresponding aligned vector at this new location is obtained trough bilinear interpolation. Because of the curvature of the geopotential isolines, the original ~~and the 5-km shifted vectors~~ vectors and those shifted by 5 km are rotated against each other, and it is the angle between these two ~~vectors~~ vectors – normalized by the distance of 5 km – that we define as the local curvature. The curvature field $\alpha(x, y)$ is available on the whole global grid and is used to identify the trough and ridge objects. These steps are summarized in Fig. 2.

To identify troughs and ridges, a threshold of $5 \cdot 10^{-5}$ ~~degree~~ degrees per meter is used to mask the curvature field (Fig. 1b). This threshold is the main degree of freedom of the algorithm. All connected points in the masked field, which form a coherent object, are clustered into one distinct 2D trough or ridge depending on the sign of the curvature field (Fig. 1c). Grid points outside a coherent object are flagged with zeros, grid points insides with ones. Time-averaging over the obtained binary fields yields detection frequencies, which indicate the fraction of time steps affected by a trough or ridge relative to all time steps. We selectively disregard very small features ($<$ ~~$20 \cdot 111^2$ km~~ $< 20 \cdot$ [111 km]^2), which at this stage ~~unlikely~~ are unlikely to correspond to a significant flow deviation. Additionally, consideration is only given to midlatitude troughs and ridges within 20°~~S–70~~N–70°N, but the algorithm in general could be applied also to polar latitudes. Figure 1 illustrates the individual steps ~~. Figure~~ in more details. Figure 1b shows the trough and ridge objects after masking the normalized curvature field using the above threshold. The trough over the eastern North Atlantic is connected to a mature low-pressure system, which is discernible from the closed ~~500 hPa~~ 500 hPa isolines in the upper-left corner of Fig. 1a and which is also well-marked at the surface. This trough is classified as a "closed trough". On the other hand, the trough object over the Central Mediterranean is not associated with a low-pressure system and is therefore classified by the algorithm as an "open trough". We decided to classify regions inside closed geopotential contours not as part of a trough or ridge object ~~, –~~ as is the case for the trough over the Atlantic in Fig. 1b ~~, –~~ but rather flag the region inside a closed geopotential contour as a distinct low- or high-pressure ~~systems~~ system, as in Sprenger et al. (2017). In this way, troughs and ridges can be classified as either independent of, or as linked with, a low- or high-pressure system; and the troughs and ridges are classified as such by the algorithm.

In a final step, the corresponding trough and ridge axes are identified. The result of this step is shown in Fig. 1d. Algorithmically, a starting point is first selected within each 2D trough and ridge object~~, and~~ ; we decided to start at the highest (for troughs) and lowest (for ridges) geopotential value within each object. From this starting point, a line is iteratively constructed by stepping 5 km forward parallel to the geopotential gradient. The iterative extension of the axis line ends as soon as ~~the line~~ it leaves the 2D trough or ridge object. If the identified axis is shorter than 500 km, the axis and the corresponding 2D trough or ridge object are removed~~, which~~ . This minimum length is the second degree of freedom in our algorithm that the user

can adjust. The final outcome of the trough and ridge identification is therefore a gridded field, corresponding to the original input grid, on which trough and ridge grid cells are ~~labelled~~ labeled and flagged in different ways (e.g., open or closed). For plotting purposes, it is convenient to transform the axes into 1D polylines by means of a cubic-spline interpolation (as is done in Fig. 1e,f).

The troughs and ridges are further characterized with respect to their horizontal orientation. The horizontal orientation (or tilt) of a trough or ridge differs from the curvature of the geopotential isolines. To obtain ~~the horizontal orientation~~it, the angle of the trough or ridge axis is estimated relative to a north-south meridian at every grid point and projected laterally to the whole 2D object. We refrain from attributing ~~an~~ a unique orientation to the entire 2D trough or ridge object. Instead, the orientation can change, or even reverse its sign, along the axis of a trough or ridge. An example is shown in Fig. 1f. A positive angle corresponds to a southwest-northeast orientation (anticyclonic)~~and negative values~~ , a negative angle to a southeast-northwest orientation (cyclonic), and the orientation can change within the same object. Near-zero values correspond to meridionally oriented troughs and ridges. For instance, the southeast-northwest oriented trough in the North Atlantic is tilted cyclonically by 30–45° relative to the north-south meridians (Fig. 1f). On the other hand, the ridge to the south of the ~~UK~~ British Isles is very weakly tilted relative to the meridians, and marginally changes its orientation from its northern to its southern tip. The easternmost trough over the Central Mediterranean has a mild anticyclonic orientation (blue shading in Fig. 1f).

Finally, we apply a tracking algorithm to determine the age and overall lifetime of the individual trough and ridge objects. An example is shown in Fig. 1e, where the trough over the eastern North Atlantic is found to be rather young (6–12 h) ~~, but still~~ – a little older ~~(0–6 h)~~ than the trough over the Central Mediterranean ~~. The~~ (0–6 h), but younger than the ridge to the south of the ~~UK is about 18-24~~British Isles (18–24 h~~old~~). Algorithmically, the tracking determines ~~spatio-temporally connected trough and ridge objects by applying an overlap criterion.~~ temporal connections between trough or ridge objects while naturally accounting for mergings and splittings. The connections between two consecutive time steps are found as follows. First, each object at either time step is paired with each unique combination of up to three overlapping objects at the other time step. For example, if object $A(t_i)$ at time step t_i overlaps objects $B(t_j)$ and $C(t_j)$ at t_j, three connections are possible: $A(t_i) \rightarrow B(t_j)$, $A(t_i) \rightarrow C(t_j)$, and $A(t_i) \rightarrow B(t_j) + C(t_j)$, whereby the latter would constitute a splitting for $t_j > t_i$ and a merging for $t_i > t_j$. Second, each of these potential connection is assigned a probability, which is high if the combined object size at the two time steps is similar and the involved objects exhibit substantial overlap over time. Third, the final connections are selected iteratively in descending order of probability, whereby each object can only be part of one connection. Objects for which no connection is found constitute the beginning or end of a track (or branch thereof). Further details can be found in ~~(Rüdisühli, 2018). The tracking can~~ Section 2.2 of Rüdisühli (2018). We use the tracking to identify young troughs or ridges, but it could also be used, for example, to study the change in the orientation of the troughs and ridges during their life cycle.

2.2 Illustrative case: Downstream development over the North Atlantic–Mediterranean sector

~~In the~~ In this section, an illustrative example is briefly discussed. Figure~~2~~ 3 compares two distinct time instances (06 UTC and 12 UTC on 12 January 2010, in Fig. ~~2a~~ 3a and b, respectively) for a synoptic evolution over the eastern North Atlantic–Mediterranean sector. At 06 UTC on 12 January 2010 (Fig. ~~2a~~ 3a), a trough ~~, –~~ which is connected to a mature low-pressure

system over the eastern North Atlantic ~~,~~ is located near 20°W. Quasi-geostrophic (QG) forcing for downward motion ~~is found upstream~~ (yellow contours in Fig. ~~2)~~ 3) is found upstream of the trough axis, and forcing for upward motion ~~on its downstream side~~ (green contours in Fig. ~~2) . The quasi-geostrophic forcing~~ 3) on its downstream side. The forced omega is computed at 500 hPa according to the Q-vector formulation of the classical quasi-geostrophic omega equation ~~details of this computation are given in the supplement to Graf et al. (2017)~~in pressure coordinates,

$$\sigma\nabla^2\omega + f_0^2\frac{\partial^2\omega}{\partial p^2} = -2\nabla\cdot\mathbf{Q}\,, \tag{1}$$

where σ denote the static stability, f_0 the Coriolis paramter, ω the vertical motion and $\mathbf{Q}$ the Q-vector. For details of the derivation we refer to Holton (2004), and for details of this computation we refer to the supplement of Graf et al. (2017). The identified trough axis sits in the transition zone between downward and upward forcing, ~~thus~~ highlighting the physical relevance of the identified axis, and therefore could be used to separate the pre-trough ~~sector~~ from the post-trough sector. A downward and upward QG-forcing pattern is also discernible over the Central Mediterranean, but a corresponding trough axis is missing at 06 UTC (Fig. ~~2a~~ 3a), which is related to the degree of freedom the user has in setting the minimum curvature and length of the axis. Six hours later, at 12 UTC (Fig. ~~2b~~ 3b), the trough axis is identified and located ~~in between~~ in-between the upward and downward forcing. Overall, the temporal evolution of the synoptic situation is reminiscent of the situations discussed by Raveh-Rubin and Flaounas (2017). It seems to follow a common pattern for Mediterranean cyclogenesis~~.~~: The outflows of warm conveyor belts from ~~upstream cyclones~~ upstream-cyclones over the Atlantic Ocean tend to amplify a ridge over the eastern Atlantic~~. The~~ , and the consequent downstream wave development intrudes the Mediterranean in southern latitudes~~and provokes~~ , provoking cyclogenesis. Interestingly~~here it is a trough over the North Atlantic and the~~ , the ridge downstream already exists for a longer time period than the up- and downstream troughs. This tends to be in agreement with the finding in Raveh-Rubin and Flaounas (2017) that a series of Atlantic cyclones is necessary to initiate Mediterranean cyclogenesis. The trough and ridge tracking could ~~therefore~~ be used to quantify the time between the formation of the upstream Atlantic trough, the downstream ridge, and the downstream Mediterranean trough, plus the typical orientation of these features preceding Mediterranean cyclogenesis.

3 Climatologies

In this section, the trough and ridge diagnostics presented above are applied to compute climatologies for the extended winter (Nov–Mar) and summer (May–Sep) seasons 1979–2018 in the Northern Hemisphere. We restrict the discussion for practical reasons to the extended winter and summer seasons and the 500 hPa level, as we intend to present an in-depth discussion of the monthly and seasonal cycles in both hemispheres in future publications. The results for the 300 hPa level are shown in the supplement.

3.1 Extended Winter (November–March)

In Fig. 4a, a summary is given for the frequency of trough ~~detection, the averaged~~ objects, the frequency of incipient trough age (yellow ~~and red contours~~ contour in Fig. 4a), and the mean horizontal orientation (Fig. 4b) ~~on~~ at the 500 hPa level. During winter, the trough detection frequency displays four centers of action around the Northern Hemisphere, for example ~~,~~ over North America downstream of the Rocky Mountains ~~and over East Asia~~ – a well known surface cyclogenesis region (e.g., Bannon, 1992; Hobbs et al., 1996; Hoskins and Hodges, 2002) – and downstream of the ~~Atlai-Sayan and Yablonoi mountain ranges~~Altai. The trough detection frequency also peaks at the end of the North Pacific storm track over the Bay of Alaska~~and~~, in agreement with climatologies of surface cyclones (Fig. 4a in Wernli and Schwierz, 2006), cyclolysis (Fig. 5d in Hoskins and Hodges, 2002) and PV streamers on several isentropic levels (310–330 K in Fig. 3 in Wernli and Sprenger, 2007). It also peaks over Eastern Europe ~~slightly~~ to the north of the Black Sea, which is seen in streamer climatologies at lower isentropic levels (310 K in Fig. 3b of Wernli a . The latter maximum has an upstream branch into the Mediterranean and a downstream branch into the Caspian Sea. Surprisingly ~~, –~~ and in contrast to the Rocky Mountains ~~, –~~ there is no peak downstream of Greenland, which is an important surface cyclogenesis region. Greenland surface cyclogenesis is typically preceded by an ~~eastward propagating~~ eastward-propagating upper-level trough-ridge train, which is seen, for example, in Fig. 4 of Schemm et al. (2018). Because detection frequencies tend to highlight regions where troughs are stationary, it seems as if troughs downstream of Greenland are more transient compared to their counterparts downstream of the Rocky Mountains. Indeed, the mean lifetime of troughs is lower at Greenland compared to downstream of the Rocky Mountains (Supplementary Fig. S4) Furthermore, there is no center of action over the Nordic Seas, which is one exit region of the North Atlantic storm track. This is in contrast to the exit of the North Pacific storm track and the maximum over the Bay of Alaska.

The ~~mean trough age is~~ trough frequencies of incipient troughs are obtained using the tracking capability of the algorithm (section 2). ~~Early troughs, with an age between 0 and 1 day~~ To this end, all trough objects that are older than one day are removed from the data, and the detection frequencies of these early troughs are re-computed based on the remaining trough objects. These incipient troughs (yellow contour in Fig. 4a ~~), are most~~ indicates half of the maximum value in early-trough detection frequency) are frequently detected downstream of the Rocky Mountains and ~~over East Asia~~ downstream of the ~~Yablonoi mountain range~~Altai, suggesting that these two regions are preferred trough genesis regions. There is also a smaller peak in the ~~early trough~~ early-trough frequency near Greenland, suggesting that trough genesis also occurs ~~in~~ near Greenland. However, the reduced trough frequency compared to the Rocky Mountains suggests that Greenland troughs are indeed more transient. A second small peak of early troughs is seen in the Gulf of Genoa, a preferred ~~surface cyclogenesis~~ region for Mediterranean ~~cyclones~~cyclogenesis (Trigo et al., 2002). There are two additional, broader regions where early troughs are frequent ~~. The~~ and not linked to orography: the end of the storm track over the North Pacific, and over parts of Northern Europe ~~encompasses a broader region that extends from the UK eastward across~~ extending from the British Isles eastward across Central Europe into Russia. It is plausible to think of these early troughs over Europe as a result of synoptic systems that decay upstream over the ~~Eastern~~ eastern North Atlantic. Wave breaking and consecutive downstream developments at the end of a synoptic wave life cycle over the ~~Eastern~~ eastern North Atlantic provide then the seed for trough genesis further

downstream over Europe. ~~A~~ Finally, a note of caution regarding the climatological trough age ~~must be mentioned: to~~ is in order. To obtain the age climatology, the age information obtained from the trough tracking is assigned to every grid point inside a two-dimensional trough ~~feature. All the grid points outside a trough feature~~ object, while points outside are labeled as missing data. Time averaging of this field results in the mean age at each grid point. The climatological age is therefore a function of the trough size, and the age contours therefore enclose smaller regions ~~everywhere~~ where troughs tend to be small. Furthermore, the number of troughs at each grid point varies according to the trough frequency (color shading in Fig. 4a)~~,~~; and near the lateral boundaries of the domain, a very low number of troughs dictates the climatological mean. Late-trough frequencies typically encompass larger regions and extend further downstream (not shown), but the absolute frequency values are considerably reduced.

The trough orientation displays a strong zonal asymmetry. Over the main oceanic storm tracks, the mean trough orientation is preferentially cyclonic (blue shading in Fig. 4b). The cyclonic orientation increases ~~towards~~ toward the end of the storm tracks and ~~increases~~ also with latitude. Over land, the trough orientation is preferentially anticyclonic. The anticyclonic orientation increases ~~towards~~ toward lower latitudes. This meridional dependence of the mean trough orientation is in agreement with the conventional interpretation of cyclonic and anticyclonic wave life cycles and the associated wave breaking, which occurs poleward (cyclonic) or equatorward (anticyclonic) of the mean jet position (Thorncroft et al., 1993). Over Northern Africa, the climatological trough orientation is strongly anticyclonic. In this region, troughs are frequently associated with anticyclonic ~~waves~~ wave breaking downstream of a mature extratopical cyclone situated off the Iberian Peninsula. This downstream trough eventually thins and elongates equatorward, corresponding to PV streamer formation. Eventually, an upper-level cutoff low ~~will form later~~forms. From the perspective of Rossby wave packets propagating along wave guides, the anticyclonic troughs in this sector have been described as the transmitters between wave packets initiated on the subtropical wave guide (i.e., the jet over Northern Africa) by wave packets that propagate along the extratropical wave guide over the North Atlantic ~~(Martius et al., 2010, ;in particular Fig. 5)~~(Martius et al., 2010, in particular their Fig. 5).

In Fig. 5a, a summary is given for the number of ridges detected during the cold season. Remarkably, the ridge detection frequency over many regions is larger by almost a factor of two compared to the trough detection frequency. For example, the ridge detection frequency downstream of Greenland with a preferred cyclonic orientation (Fig. 5b) is ~~as~~ twice as high as that for troughs. The band of enhanced ridge frequencies elongates downstream over the Nordic Seas, peaks over the Scandinavian Mountains and remains on a relatively high level over Siberia. Upstream of the ~~Atlai-Sayan and Yablonoi Mountains~~Altai, the ridge frequency decreases~~,~~, while downstream, the trough frequency peaks (Fig. 4a). Over large parts of Siberia, the ridges have no preferred orientation, while they tend to be anticyclonically oriented over East Asia. This band of higher ridge frequencies might relate to the Siberian storm track ~~,~~– seen in the track densities of ~~250-hPa~~ 250 hPa meridional wind anomalies (Fig. 4a in Hoskins and Hodges, 2019) ~~,~~– while the main surface storm track is located further poleward over the Barents Sea region ~~(Fig. 4a Wernli and Schwierz, 2006)~~(Fig. 4a in Wernli and Schwierz, 2006). Over East Asia and the ~~West~~ western Pacific, the ridge detection frequency is rather low, while the climatology ~~is dominated by stationary ridges~~ over the Coast Mountains of western North America ~~,~~ is dominated by stationary ridges which preferentially have a cyclonic orientation (blue shading in Fig. 5b). A smaller region of high early-age ~~trough~~ ridge frequencies is found near Kamchatka (yellow contour in Fig. 5a),

which indicates the presence of a transient ridge with a preferred cyclonic orientation (blue shading in Fig. 5b). Indeed, a local maximum in the surface cyclone frequencies is found downstream of Kamchatka (see Fig. 4a in Wernli and Schwierz, 2006). Overall, the trough and ridge pattern alternates almost periodically in terms of the amplitude around the Northern Hemisphere.

We further explored the role of the level and the minimum lifetime of the detected features on the trough and ridge frequencies. The trough and ridge detection patterns and the corresponding orientation at the 300 hPa level are in very close agreement with the results at the 500 hPa level (Supplementary Fig. S1). The detection frequencies are increased everywhere by 10–20 %, but the main centers of action and the mean orientation agrees well between the levels. We further computed the climatologies after removing short-lived features that have a maximum lifetime of 24 hours in a post-processing step (Supplementary Fig. S3). Again, the resulting patterns parallel those shown in Fig. 4 and Fig. 5, but the detection frequencies are reduced.

3.2 Extended Summer (May–September)

The pattern in the trough detection frequencies changes from winter to summer (Fig. ~~3c~~ 4). Over North America, the main frequency peak is located downstream of the Great ~~Lake~~ Lakes Region and over Newfoundland, while it was previously located further upstream. This is in agreement with the high surface cyclone frequencies seen in summer in this region (see Fig. 4c in Wernli and Schwierz, 2006). Over the North Atlantic, the main frequency peak is located just off the Iberian Peninsula. There is no comparable peak in surface cyclone frequencies in this region, so the flow conditions will result in the formation of a cut-off low with no well-marked surface signature. Surface cyclone frequencies have a peak downstream of Greenland (see Fig. 4c in Wernli and Schwierz, 2006)~~; however, ,~~ but there is no maximum trough frequency there. However, upper-level storm-track measures ~~, –~~ based on, for example, track densities of 250 hPa vorticity ~~, –~~ indeed indicate the presence of a trough-like feature off the Iberian Peninsula during summer (see Fig. 1c in Hoskins and Hodges, 2019). Because a similar feature is also seen in summertime climatologies of Rossby wave breaking (see Fig. 10a in Postel and Hitchman, 1999), we expect this maximum in trough frequency to be related to anticyclonic ~~Rossy~~ Rossby wave breaking as described for the LC1 scenario in Fig. 12a of Thorncroft et al. (1993). An example of such a synoptic situation is also shown in Fig. 5.7 of Martius and Rivière (2016).

Over Eurasia, ~~one~~ a maximum in the summertime detection frequencies of troughs connects the Eastern Mediterranean with the Black Sea. This feature is not well reproduced in Rossby wave breaking climatologies of which we are aware, but it is clearly seen in the upper-level track densities in vorticity on 250 hPa (Hoskins and Hodges, 2019). Furthermore, this local maximum corresponds to a similar maximum seen in summertime climatologies of stratospheric PV streamers (see Fig. 6b in Wernli and Sprenger, 2007). ~~Streamers~~ PV streamers form a subcategory of troughs and are best described as filament-like elongated troughs, which have a length that is longer than their width (Wernli and Sprenger, 2007). Streamers are associated with anticyclonic Rossby wave breaking, so it is not too surprising that the detection hot spots off the Iberian Peninsula and near the Black Sea eventually become part of the same Rossby wave train [see for example Fig. ~~–~~ 3 in (Wernli and Sprenger, 2007) for such a synoptic situation]. A second maximum over Eurasia is located ~~near Lake Baikal~~west of 90°E, a feature seen again in the streamer climatology of Wernli and Sprenger (2007). Further east, the maximum over East Asia exhibits only weak changes in its location between winter (Fig. ~~2a~~ 4a) and summer (Fig. ~~2c~~ 4c) but appears with a reduced amplitude

during summer. Finally, over the ~~East North~~ northeastern Pacific, the summer maximum is ~~located~~ shifted slightly equatorward compared to its position during winter. It is located off the ~~West Coast of the US~~ US west coast during summer, while it is located in the Bay of Alaska during winter. This is a ~~counterintuitive~~ counter-intuitive result because storm tracks generally tend to shift poleward during summer (Hoskins and Hodges, 2019).

The ridge frequency pattern over North America continues to be dominated by the stationary ridges over the Coastal Mountains despite a mild reduction in the absolute detection ~~values~~ frequencies (color shading in Fig. 5c).

Finally, we note that – as is the case for the winter season – the results obtained at the 300 hPa level (Supplementary Fig. S1) are in very close agreement with those at the 500 hPa level. The 300 hPa detection frequencies are moderately higher, but the patterns are remarkably similar.

3.3 ENSO-affected winter seasons

The influence of the ~~El Niño–Southern Oscillation (ENSO)~~ ENSO on the midlatitudes is a longstanding research topic – for recent reviews, we refer the reader to publications by Liu and Alexander (2007); Stan et al. (2017) and Yeh et al. (2018). Recently, ~~progress has particularly~~ particular progress has been made in understanding the role of synoptic-scale eddies in shaping the North Atlantic circulation response to ENSO. More specifically, there is increasing evidence that the North Atlantic teleconnection pattern is in part a downstream response of the eddy-driven jet to changes in the orientation of synoptic-scale eddies entering the North Atlantic from North America (Li and Lau, 2012a, b; Drouard et al., 2015). The mechanisms can be briefly summarized as follows – for a schematic summary see also Fig. 13 in Schemm et al. (2018): In response to an amplified ridge over the northeastern Pacific during La Niña, upper-level synoptic eddies with a more anticyclonic orientation form downstream of the Rocky Mountains, where lee cyclogenesis is also enhanced. These eddies propagate downstream over the North Atlantic while maintaining their anticyclonic orientation until anticyclonic wave breaking occurs over the eastern North Atlantic. Anticyclonic wave breaking pushes the eddy-driven jet poleward. Until now, the anomalous anticyclonic orientation and the associated more poleward eddy momentum flux were diagnosed using the horizontal **E** vectors of Hoskins et al. (1983) and Trenberth (1986), which are obtained using high-pass filtered wind data~~.~~,

$$\mathbf{E} = \begin{bmatrix} \frac{1}{2}\left(\overline{v^{*2} - u^{*2}}\right) \\ -\overline{u^* v^*} \end{bmatrix}, \tag{2}$$

where the overbar indicates a time average, and the asterisks a deviation from the time average. The fundamental relationships between the trough and ridge orientation and the eddy momentum flux have been discussed as early as by Jeffreys (1926) and Starr (1948). As summarized in the introduction, equatorward-pointing **E** vectors are assumed to indicate anticyclonically oriented eddies (Rivière et al., 2003) associated with a more poleward eddy momentum flux. During El Niñoño, the situation is essentially the opposite: Eddies downstream of the Rocky Mountains exhibit a more cyclonic ~~tilt~~ orientation and tend to push the North Atlantic jet equatorward, as is suggested by more poleward-oriented **E** vectors. The Pacific and North Atlantic jets are more zonally extended, which tends to increase extratropical cyclogenesis over the Gulf Stream (Schemm et al., 2016). To

shed further light on this, we therefore explore the ENSO climatologies using ~~trough and ridge detection~~troughs and ridges, which are very closely related to the upper-level eddies described above.

In Fig. 6, anomalies in the orientation of troughs and ridges are shown for ENSO-affected winter seasons based on the Oceanic Niño Index (ONI) from NOAA's Climate Prediction Center. During El Niño (Fig. 6a), troughs and ridges exhibit a stronger cyclonic orientation over the northeastern ~~North~~ Pacific, North America and ~~over~~ the North Atlantic. The anomalies are strongest over the northeastern Pacific ~~off the East Coast~~ and off the east coast of the US. Over the North Atlantic, the stronger-than-usual cyclonic orientation is most pronounced along 30°N, which is about the latitude of the zonally more extended jet in this region during El Niño. In contrast, during La Niña, troughs and ridges exhibit a more anticyclonic orientation over the ~~eastern North~~ northeastern Pacific, North America and parts of the North Atlantic. These results are in agreement with those from ~~previous studies, which~~ the previous studies that rely on the strength and orientation of the **E** vectors. The results are also in good agreement with the findings of Shapiro et al. (2001), who noted more life cycles of type LC2 (cyclonic) over the Pacific during El Niño and more life cycles of type LC1 (anticyclonic) during La Niña. The trough and ridge detection and tracking algorithm can thus enrich insights into the dynamics of upper-level eddies during ENSO-affected winters. For example, the anomalies during El Niño over the northeastern Pacific are predominantly due to more cyclonically oriented troughs, while the anomalies over the North Atlantic have a stronger signal in the ridge anomalies (not shown). The more cyclonic trough and ridge orientation over the Pacific is connected to the deepening of the Aleutian ~~Low~~ *Low* during El Niño, whereas it is a strong Aleutian ~~High~~*High* during La Niña, which is in agreement with more anticyclonic troughs and ridges (Mo and Livezey, 1986).

3.4 The North Pacific storm track in midwinter

The midwinter suppression of the North Pacific ~~storm-track~~ storm track intensity is another research topic that has recently received renewed attention. While the mean baroclinicity is largest during midwinter, storm track activity is reduced over the North Pacific ~~,~~ – in contrast to the North Atlantic (Nakamura, 1992). ~~Feature-based~~ As feature-based tracking statistics have shown~~that~~ , the suppression is connected to a reduced eddy intensity and upper-level eddy frequency (Penny et al., 2010), while it does not affect the frequency of surface eddies (Schemm and Schneider, 2018). Several mechanisms ~~are~~ have been suggested to contribute to the suppression~~. For example,~~ , for example a reduction in upstream seeding ~~was strongly debated (Penny et al., 2010; Chang and Guo, 2011; Penny et al., 2011; Chang and Guo, 2012; Penny et al., 2013), as well as~~ (Penny et al., 2010; Chang and Guo, 2011; Penny et al., 2011; Chang and Guo, 2012; Penny et al., 2013), or an increase in the jet speed ~~and~~ with a concomitant reduction in the jet width (Harnik and Chang, 2004). Recently, however, several studies have highlighted the important role of processes internal to the North Pacific storm track, such as a reduction in the lifetime of eddies (Schemm and Schneider, 2018) and an increase in the eddy group velocity (Chang, 2001). There is growing evidence that the equatorward shift in the subtropical jet is key for understanding the suppression (Chang, 2001; Nakamura and Sampe, 2002; Yuval et al., 2018; Schemm and Rivière, 2019). When the subtropical jet over the Pacific shifts equatorward, the efficiency of synoptic systems to convert the mean baroclinicity into eddy energy is reduced due to a change in the vertical eddy structure (Chang, 2001; Schemm and Rivière, 2019). The vertical eddy structure ~~,~~ – which is more poleward when the eddy efficiency decreases during midwinter ~~,~~ – is constrained by the eddy propagation direction, which is more ~~towards~~ shifted toward the

equator during midwinter (Schemm and Rivière, 2019; Novak et al., 2020) ~~;~~ – see, for example, Figs. 1 and 8 in Schemm and Rivière (2019). Equatorward jet shifts also reduce the storm-track intensity over the North Atlantic (Penny et al., 2013; Afargan and Kaspi, 2017)~~and even~~ . This is also the case in idealized aqua-planet simulations (Novak et al., 2020).

The equatorward shift of the Pacific jet changes the large-scale environment in which synoptic systems grow because more systems will ~~now~~ grow on the poleward flank of the jet. The poleward flank is characterized by a large-scale ~~cyclonic-sheared~~ cyclonically sheared environment. According to idealized wave life cycles (Thorncroft et al., 1993), we must expect more cyclonic (LC2) developments during midwinter. Indeed, troughs and ridges at the ~~500-hPa~~ 500 hPa level exhibit a stronger cyclonic orientation ~~during~~ in January (Fig. 7b) compared to, for example, November and April (Fig. 7a,c). Not only ~~increases~~ does the mean cyclonic orientation ~~during midwinter~~ increase during midwinter, but also wider parts of the Pacific are ~~now~~ affected by cyclonically oriented troughs and ridges. In particular, ~~during~~ in January, cyclonic troughs ~~dominated~~ dominate the North Pacific even equatorward of 40°N, which is not the case ~~during~~ in November and April.

There are several observations based on trough and ridge detection that may prove useful in gaining a better understanding of the midwinter suppression. First, there is no marked reduction in the ~~number~~ frequency of troughs and ridges during midwinter, ~~which, however,~~ as is the case for bandpass-filtered eddies at the same height (Penny et al., 2010). ~~Second, there is basin-wide dominance of cyclonically oriented troughs (and, to a lesser extent, ridges)~~ A local increase in trough frequency over the eastern Pacific is observed (yellow contours in Fig. 7d) and an overall poleward movement of the ridge frequencies, which otherwise do not display a well-marked reduction. Second, the preferred trough and ridge orientation is cyclonic during midwinter, with two maxima over the eastern ~~Pacific~~ and western Pacific (right column in Fig. 7b), which indicates a consistent change in the character of synoptic wave life cycles during midwinter. The first maximum between 40–50°N, 165°–180°E is ~~colocated~~ collocated with the region of maximum reduction in the efficiency of baroclinic growth (see Fig. 2b in Schemm and Rivière, 2019) and slightly upstream of the maximum in eddy kinetic energy (see Fig. 1 in Schemm and Schneider, 2018), which is suppressed during midwinter. Because the cyclonic orientation of troughs and ridges is typically strongest during the final stage of a synoptic wave life cycle, a plausible ~~,~~ – but here untested ~~,~~ – hypothesis for the existence of the first maximum would be that synoptic cyclones generated east of Japan over the Kuroshio extension have an accelerated life cycle with a fast and intense deepening phase followed by a rapid decay~~.~~ , resulting in a reduced life time as found by Schemm and Schneider (2018) . The enhanced lysis over the eastern Pacific is in agreement with the localized trough frequency maximum (yellow contours in Fig. 7d), because – as was shown in a previous section – maxima in the trough frequency exhibit a strong agreement with maxima in cyclolysis (compared with, for example, Fig. 5d in Hoskins and Hodges, 2002). Thus, the conversion rates and ~~EKE~~ eddy kinetic energy (EKE) are reduced downstream of the maximum cyclonic orientation of the upper-level troughs compared to the shoulder seasons. Indeed, a reduction in the lifetime of synoptic systems is observed during midwinter (Schemm and Schneider, 2018). The second maximum is related to the decay of the synoptic waves at the exit of the Pacific storm track in the Bay of Alaska.

4 Lagrangian perspective on troughs and ridges

In this section, we show how trough and ridge detection can be used to investigate trough and ridge dynamics from a Lagrangian perspective. To this end, we couple the trough and ridge detection ~~tool with the Lagrangian analysis tool~~ with a Lagrangian analysis using LAGRANTO [Wernli and Davies (1997); Sprenger and Wernli (2015)], which we use to compute air parcel trajectories from detected trough and ridge features.

The procedure is best explained ~~using~~ with a simple example ~~.~~ (Fig. 8). At 18:00 UTC on 18 ~~Jan~~ January 2010, a trough is detected over the Nordic Seas downstream of a mature low-pressure system south of Greenland (Fig. 8a). The trough has a ~~mild~~ mildly cyclonic orientation and will broaden during the following days. A potential research question ~~would~~ may be: Is the formation of this downstream trough predominately driven by dry dynamics or considerably modified by diabatic processes? ~~Parcel~~ To answer this, air parcel trajectories are released from every grid point inside the trough feature (thin gray lines in Fig. 8a), which highlight the pathway of air parcels that constitute the trough at the ~~500 hPa~~ 500 hPa level. The mean ~~evolution~~ evolutions of pressure (Fig. 8b) and ~~potential vorticity~~ PV (Fig. 8c) along these parcel trajectories ~~suggests~~ suggest that the air is mostly advected horizontally with ~~only small~~ a minor descent of approximately 20 hPa in 24 h. Further, the diabatic modification of ~~the potential vorticity~~ PV during the 24~~hours~~ h prior to arrival in the target region ~~. The potential temperature~~ is small. The mean potential temperature (not shown) decreases during this period ~~only marginally~~ from 297 K to 295 K. While the mean values suggest only little change in pressure and PV, the histograms of 24 h changes in pressure and PV show that around 15 % of the air descends during the 24 h period by up to 60–80 hPa (Fig. 8d), and that a small fraction of less than 5 % decrease their PV by more than 0.4 pvu[1] (Fig. 8e). Thus, the dynamics underlying the formation of this specific downstream trough ~~are,~~ at this stage of its life cycle ~~, mostly dry~~are mostly dry, and therefore can be ~~understood~~ approximated by the traditional paradigm of downstream development (Simmons and Hoskins, 1979; Orlanski and Chang, 1993; Simmons, 1994; Papritz and Schemm, 2013). However, for a small embedded fraction of air, much stronger descent and diabatic PV modifictation than indicated by the mean are observed.

Next, ~~24-hour~~ 24 h backward trajectories are released from all ~~the~~ detected troughs and ridges over the North Atlantic (60°–0°W, 20–70°N) in one winter ~~(January 2010) and in~~ and one summer month~~(July 2010). During~~ : January 2010, when more than 25,000 parcel trajectories are released~~, and during~~ ; and July 2010 ~~,~~ with more than 16,000 parcel trajectories. The binned ~~24-hour~~ 24 h changes for pressure~~and potential vorticity~~ , potential vorticity and potential temperature are presented in Fig. 9. During January 2010, the distribution of ~~24-hour~~ 24 h pressure changes is centered between ~~0-100~~ 0–100 hPa (corresponding to a weak descent) and is highly skewed ~~towards~~ toward negative values (corresponding to a strong ascent) of up to -500 hPa, ~~while positive values are capped at~~ in contrast to positive values which do not exceed 250 hPa. This phenomenon reflects the nature of the ~~mean isentropic~~ air mass motion inside troughs in which ~~equatorward pushing~~ equatorward-moving air mildly descends due to ~~isentropic~~ the quasi-isentropic downglide, while ~~for~~ in some cases vigorous vertical motions occur ~~, which is~~ – in agreement with the long tail ~~towards~~ toward positive values of the potential temperature distribution (Fig. 9e,f~~,). The~~). We refer to the descending motion as quasi-isentropic, because for most trajectories a mild decrease in potential temperature between -2 K and

[1] 1 pvu $= 10^{-6}\,\mathrm{m^2\,s^{-1}\,K\,kg^{-1}}$

0 K is found, likely resulting from radiative cooling. Most of these air parcels are associated with only small changes in pressure. The overall asymmetry in the pressure change distribution ultimately relates to the occurrence of upward moist convection and the impact of condensation on the vertical motion in the atmosphere. This skewness is thus a general feature of extratropical cyclones in a moist atmosphere (O'Gorman, 2011). The skewness and asymmetry is assumed to increase in a warmer climate and with increasing moisture content (Booth et al., 2015; Tamarin-Brodsky and Hadas, 2019; Sinclair et al., 2020). The trajectories associated with strong vertical motion all originate in the boundary layer and first increase and later decrease their potential vorticity (not shown), which is characteristic of a warm conveyor belt ascending ahead of the trough axis (e.g., Wernli and Davies, 1997). These cases exhibit a marked increase in potential temperature, which reflects the cross-isentropic motion. For the few cases with a strong decrease larger than 200 Pa in 24hours h, we find that the vast majority most of the parcels , which originate from levels between 200 and 300 originating between 200–300 hPa ,– decrease their potential vorticity. Only a small fraction of approximately 1% starts with stratospheric values (>2 pvu[2]), but we assume that this number increases for 300-hPa troughs. The binned 24-hour changes of potential temperature are centered between -2 and 0300 K. Most of these air parcels are associated with only a mild change in pressure. Our interpretation is that the reduction in potential temperature is due to radiative cooling, but a detailed analysis of all diabatic tendencies would be needed to confirm this result. hPa troughs. Finally, we note that the 24-h 24 h pressure change for July is even more confined to values between 0 and 1000–100 hPa, while the 24-h 24 h change in potential vorticity is more confined between -0.2 and 0.2 pvu, which is a result that reflects the overall more intense cyclone and associated trough-ridge development and vertical motion during winter.

For the 500-hPa 500 hPa ridges, the histogram of changes in pressure along the flow of 24-hour 24 h backward parcel trajectories is centered between -100 and 0 hPa, again with a longer tail towards negative values . toward negative values (Fig. 10). It is therefore shifted more towards toward negative values than the trough histogram, which reflects the isentropic quasi-isentropic upglide of air sliding moving poleward and upward in a ridge. The pressure change during in July is again more shifted towards toward negative values (ascent) than the trough histogram but is centered around -50–50-50 and 50 hPa. If our interpretation is correct, the histograms are dominated by the mean mostly dry almost isentropic motion of air inside troughs and ridges, and the reduced pressure change along the flow in July relative to January reflects the reduced baroclinicity or isentropic tilt in summer compared to winter–, in combination with a reduced wind speed according to the thermal wind relationship. It is, however, important to note that the histograms of potential temperature and vorticity changes show that the motion is not fully dry adiabatic. The histograms of potential vorticity changes are symmetrically distributed around zero with outliers on both sides of the spectrum, while the distribution of the 24-hour 24 h potential temperature changes are centered around week weak negative values (–2 to 0between -2 and 0 K), which is similar to the troughs.

5 Conclusions

In this paper, a novel method to detect the full life cycle of upper-level troughs and ridges is presented, which is computationally efficient and closes an existing gap between tools that focus either on the wave breaking phase or on the initiation phase of

[2] 1 pvu = 10^{-6} m^2 s^{-1} K kg^{-1}

upper-level Rossby waves. The presented approach is based on the curvature of the geopotential isolines at a given isobaric surface. Grid points above a predefined curvature value are grouped into two-dimensional features and labeled as trough or ridge features. The algorithm further categorizes the corresponding trough and ridge axes as line objects and identifies ~~the~~ their horizontal orientation. It also performs a spatio-temporal tracking of the identified features. The detection of the trough and ridge axes allows for the identification of pre- and post-trough~~or~~ /ridge sectors, respectively. This facilitates a variety of new applications ~~for related~~ relating troughs and ridges to other meteorological variables such as cloud types, precipitation, warm conveyor belts or jet streams. The detection of the horizontal orientation allows for the grouping of troughs and ridges into cyclonic and anticyclonic categories. The tracking ~~allows for the determination of the~~ enables determining the maturity of the troughs and ridges and ~~how~~ the orientation changes during the life cycle. Finally, the algorithm separates closed ~~troughs~~ from open troughs and ridges. The former are associated with one ~~ore~~ or more closed geopotential isolines and ~~are~~ therefore related to upper-level lows or highs, which allows ~~the possibility to connect them~~ them to be connected with surface low-pressure systems.

The second focus of this paper is on illustrating the ~~performance of the~~ detection using a case study and several climatological applications. These ~~applications~~ serve as stepping stones for future research. ~~The generalbehavior of~~ In general, the detection frequencies of both troughs and ridges ~~is that both the trough and ridge detection frequencies~~ are remarkably stationary, but regionally the picture can be complex. For example, during winter, troughs are most frequently detected downstream of the Rocky Mountains and ~~over East Asia~~ downstream of the ~~Atlai-Sayan and Yablonoi mountain ranges~~Atlai, but they are much less ~~frequently found~~ frequent downstream of Greenland ~~, where, in~~ – where, by contrast, the ridge detection frequency is high. Thus, troughs are more transient or smaller ~~in~~ near Greenland. Troughs are also frequent at the end of the Pacific storm track ~~,~~ ~~but there is no comparable frequency maximum~~ and at the end of the Atlantic storm track during winter, where the frequency maximum of incipient troughs is high over the British Isles extending over eastern Europe. Rather, a frequency maximum is located over ~~East Europe ,~~ Eastern Europe – which is in contrast to summer, when there is a clear maximum at the end of the Atlantic storm track off the Iberian Peninsula (Fig. 4 and Fig. 5).

The horizontal orientation of troughs and ridges displays a strong meridional and longitudinal dependency. In general, troughs and ridges are oriented cyclonically over the main oceanic storm tracks ~~, troughs and ridges are cyclonically oriented, while they are oriented~~ but anticyclonically over land. The cyclonic orientation increases poleward, while the anticyclonic orientation increases equatorward. In agreement with earlier findings ~~, which are~~ – based on traditional means to quantify the behavior of upper-level eddies~~(~~, such as **E** ~~vector),~~ vectors – troughs and ridges are more cyclonically oriented over North America and the North Atlantic during El Niño-affected winter seasons. ~~In~~ By contrast, these areas are more anticyclonically oriented during La Niña-affected winter seasons. Trough and ridge detection thus provides complementary insights into the change in the dynamics of the large-scale upper-level flow in response to external climate drivers ~~. However, the orientation~~ such as ENSO.

The orientation of trough and ridge axes also exhibits a seasonal cycle, for example ~~,~~ during midwinter over the North Pacific when the Pacific jet moves equatorward. The subtropical jet creates a large-scale cyclonically sheared environment over the Pacific. Consequently, the troughs and ridges ~~are during midwinter mostly cyclonic, and it is in particular the trough~~

~~orientation that has~~ during midwinter are mostly oriented cyclonically. The trough orientations in particular exhibit a marked increase in cyclonic orientation, suggesting a potentially accelerated cyclone life cycle~~. These applications give~~ , which is in agreement with an emerging trough frequency maximum over the northeastern Pacific. The latter suggests enhanced cyclolysis and wave breaking in this region. These applications serve as an indication for the usefulness of the novel detection method and complementary insights that can be gained from it.

Finally, we explored the possibility of utilizing the detected troughs and ridges as starting points for air parcel trajectories. Twenty-four-hour backward trajectories are released for two months (January and July 2010) from all the trough and ridge objects. For troughs, the distribution of ~~24-hour~~ 24 h pressure changes along the flow is centered between 0 and 100 hPa, which reflects the ~~isentropic upglide of poleward~~ near-isentropic downglide of equatorward moving air in a trough, with a long tail ~~towards~~ toward negative values (strong ascent). For ridges, the distribution is consequently centered between -100 and 0 hPa, which reflects the ~~isentropic downglide of equatorward~~ near-isentropic upglide of poleward moving air in a ridge. Again, the distribution has a long tail ~~towards~~ toward negative values. During ~~the~~ summer, the tails of both distributions are reduced and strongly centered around small pressure changes of 50 hPa. If the distributions reflect mainly the ~~mean isentropic~~ near-isentropic motion of air masses in trough and ridge regions, then the strong confinement of the summer distributions near small pressure changes is due to the reduced baroclinicity. The corresponding distribution of PV changes is centered around zero, with similar tails ~~towards~~ toward positive and negative values. Finally, the distribution of potential temperature changes is centered around negative values (between ~~−2 and 0~~-2 and 0 K~~day~~ d^{-1}), with a long tail ~~towards~~ toward positive values. While the long tail reflects the heating during rapid cross-isentropic ascent, the mean and median ~~indicates~~ indicate a mild loss potentially due to radiative cooling. Consequently, the mean motion of air in a trough and ridge is only close to isentropic, with stronger positive than negative outliers (Figs. 8e and 9e).

The presented ~~tools offer~~ tool offers new possibilities for studying the dynamics of upper-level wave development and associated meteorological conditions at the surface or at the jet stream level. ~~The~~ Their application to climate data or century-long reanalysis data will allow for the analysis of long-term trends, extreme seasons or decadal variability in the frequency and orientation of troughs and ridges. The combination of the tool with Lagrangian diagnostics will allow for the development of a new three-dimensional perspective on trough and ridge development and for a quantification of the role of moist processes in shaping their life cycle.

Code and data availability. The monthly mean data will be made available at http://eraiclim.ethz.ch/. Higher resolution data and the Fortran and Python codes can be provided upon request.

Author contributions. SeS and MS designed jointly the detection strategy. MS developed the algorithm. SR developed the tracking. SeS performed the analyses. SeS and MS contributed equally to the interpretation and discussion of the results. All authors helped to write the paper.

Competing interests. The authors declare no competing interests.

References

Afargan, H. and Kaspi, Y.: A Midwinter Minimum in North Atlantic Storm Track Intensity in Years of a Strong Jet, Geophysical Research Letters, 44, 12,511–12,518, https://doi.org/10.1002/2017GL075136, 2017.

Bannon, P. R.: A Model of Rocky Mountain Lee Cyclogenesis, Journal of the Atmospheric Sciences, 49, 1510–1522, https://doi.org/10.1175/1520-0469(1992)049<1510:AMORML>2.0.CO;2, 1992.

Benedict, J. J., Lee, S., and Feldstein, S. B.: Synoptic View of the North Atlantic Oscillation, Journal of the Atmospheric Sciences, 61, 121–144, https://doi.org/10.1175/1520-0469(2004)061<0121:SVOTNA>2.0.CO;2, 2004.

Booth, J. F., Polvani, L., O'Gorman, P. A., and Wang, S.: Effective stability in a moist baroclinic wave, Atmospheric Science Letters, 16, 56–62, 2015.

Browning, K. A.: Conceptual Models of Precipitation Systems, Weather and Forecasting, 1, 23–41, https://doi.org/10.1175/1520-0434(1986)001<0023:CMOPS>2.0.CO;2, 1986.

Browning, K. A.: Organization of Clouds and Precipitation in Extratropical Cyclones, in: Extratropical cyclones, pp. 129–153, American Meteorological Society, Boston, MA, https://doi.org/10.1007/978-1-944970-33-8_8, 1990.

Chang, E. K. M.: GCM and Observational Diagnoses of the Seasonal and Interannual Variations of the Pacific Storm Track during the Cool Season, Journal of the Atmospheric Sciences, 58, 1784–1800, https://doi.org/10.1175/1520-0469(2001)058<1784:GAODOT>2.0.CO;2, 2001.

Chang, E. K. M. and Guo, Y.: Comments on "The Source of the Midwinter Suppression in Storminess over the North Pacific", Journal of Climate, 24, 5187–5191, https://doi.org/10.1175/2011JCLI3987.1, 2011.

Chang, E. K. M. and Guo, Y.: Is Pacific Storm-Track Activity Correlated with the Strength of Upstream Wave Seeding?, Journal of Climate, 25, 5768–5776, https://doi.org/10.1175/JCLI-D-11-00555.1, 2012.

Davies, H. C., Schär, C., and Wernli, H.: The Palette of Fronts and Cyclones within a Baroclinic Wave Development, Journal of the Atmospheric Sciences, 48, 1666–1689, https://doi.org/10.1175/1520-0469(1991)048<1666:TPOFAC>2.0.CO;2, 1991.

Dee, D. P., Uppala, S. M., Simmons, A. J., Berrisford, P., Poli, P., Kobayashi, S., Andrae, U., Balmaseda, M. A., Balsamo, G., Bauer, P., Bechtold, P., Beljaars, A. C. M., van de Berg, L., Bidlot, J., Bormann, N., Delsol, C., Dragani, R., Fuentes, M., Geer, A. J., Haimberger, L., Healy, S. B., Hersbach, H., Hólm, E. V., Isaksen, L., Kållberg, P., Köhler, M., Matricardi, M., McNally, A. P., Monge-Sanz, B. M., Morcrette, J.-J., Park, B.-K., Peubey, C., de Rosnay, P., Tavolato, C., Thépaut, J.-N., and Vitart, F.: The ERA-Interim reanalysis: configuration and performance of the data assimilation system, Quarterly Journal of the Royal Meteorological Society, 137, 553–597, https://doi.org/10.1002/qj.828, 2011.

Drouard, M., Rivière, G., and Arbogast, P.: The Link between the North Pacific Climate Variability and the North Atlantic Oscillation via Downstream Propagation of Synoptic Waves, Journal of Climate, 28, 3957–3976, https://doi.org/10.1175/JCLI-D-14-00552.1, 2015.

Franzke, C., Lee, S., and Feldstein, S. B.: Is the North Atlantic Oscillation a Breaking Wave?, Journal of the Atmospheric Sciences, 61, 145–160, https://doi.org/10.1175/1520-0469(2004)061<0145:ITNAOA>2.0.CO;2, 2004.

Graf, M. A., Wernli, H., and Sprenger, M.: Objective classification of extratropical cyclogenesis, Quarterly Journal of the Royal Meteorological Society, 143, 1047–1061, https://doi.org/10.1002/qj.2989, 2017.

Grams, C. M., Wernli, H., Böttcher, M., Čampa, J., Corsmeier, U., Jones, S. C., Keller, J. H., Lenz, C.-J., and Wiegand, L.: The key role of diabatic processes in modifying the upper-tropospheric wave guide: A North Atlantic case-study, Quarterly Journal of the Royal Meteorological Society, 137, 2174–2193, https://doi.org/10.1002/qj.891, 2011.

Gray, S. L. and Dacre, H. F.: Classifying dynamical forcing mechanisms using a climatology of extratropical cyclones, Quarterly Journal of the Royal Meteorological Society, 132, 1119–1137, https://doi.org/10.1256/qj.05.69, 2006.

Harnik, N. and Chang, E. K. M.: The Effects of Variations in Jet Width on the Growth of Baroclinic Waves: Implications for Midwinter Pacific Storm Track Variability, Journal of the Atmospheric Sciences, 61, 23–40, https://doi.org/10.1175/1520-0469(2004)061<0023:TEOVIJ>2.0.CO;2, 2004.

Harrold, T. W.: Mechanisms influencing the distribution of precipitation within baroclinic disturbances, Quarterly Journal of the Royal Meteorological Society, 99, 232–251, https://doi.org/10.1002/qj.49709942003, 1973.

Hobbs, P. V., Locatelli, J. D., and Martin, J. E.: A New Conceptual Model for Cyclones Generated in the Lee of the Rocky Mountains, Bulletin of the American Meteorological Society, 77, 1169–1178, https://doi.org/10.1175/1520-0477(1996)077<1169:ANCMFC>2.0.CO;2, 1996.

Holton, J. R.: An Introduction to Dynamic Meteorology, Elsevier Academic Press, 200 Wheeler Road, Burlington, MA 01803, USA, 4th Edition, 2004.

Hoskins, B. J. and Hodges, K. I.: New Perspectives on the Northern Hemisphere Winter Storm Tracks, Journal of the Atmospheric Sciences, 59, 1041–1061, https://doi.org/10.1175/1520-0469(2002)059<1041:NPOTNH>2.0.CO;2, 2002.

Hoskins, B. J. and Hodges, K. I.: The Annual Cycle of Northern Hemisphere Storm Tracks. Part I: Seasons, Journal of Climate, 32, 1743–1760, https://doi.org/10.1175/JCLI-D-17-0870.1, 2019.

Hoskins, B. J., James, I. N., and White, G. H.: The Shape, Propagation and Mean-Flow Interaction of Large-Scale Weather Systems, Journal of the Atmospheric Sciences, 40, 1595–1612, https://doi.org/10.1175/1520-0469(1983)040<1595:TSPAMF>2.0.CO;2, 1983.

Jeffreys, H.: On the dynamics of geostrophic winds, Quarterly Journal of the Royal Meteorological Society, 52, 85–104, https://doi.org/10.1002/qj.49705221708, 1926.

Lackmann, G. M., Keyser, D., and Bosart, L. F.: A Characteristic Life Cycle of Upper-Tropospheric Cyclogenetic Precursors during the Experiment on Rapidly Intensifying Cyclones over the Atlantic (ERICA), Monthly Weather Review, 125, 2729–2758, https://doi.org/10.1175/1520-0493(1997)125<2729:ACLCOU>2.0.CO;2, 1997.

Lee, S. and Feldstein, S.: Two Types of Wave Breaking in an Aquaplanet GCM, Journal of the Atmospheric Sciences, 53, 842–857, https://doi.org/10.1175/1520-0469(1996)053<0842:TTOWBI>2.0.CO;2, 1996.

Li, Y. and Lau, N.-C.: Impact of ENSO on the Atmospheric Variability over the North Atlantic in Late Winter—Role of Transient Eddies, Journal of Climate, 25, 320–342, https://doi.org/10.1175/JCLI-D-11-00037.1, 2012a.

Li, Y. and Lau, N.-C.: Contributions of Downstream Eddy Development to the Teleconnection between ENSO and the Atmospheric Circulation over the North Atlantic, Journal of Climate, 25, 4993–5010, https://doi.org/10.1175/JCLI-D-11-00377.1, 2012b.

Liu, Z. and Alexander, M.: Atmospheric bridge, oceanic tunnel, and global climatic teleconnections, Reviews of Geophysics, 45, https://doi.org/10.1029/2005RG000172, 2007.

Martius, O. and Rivière, G.: Rossby wave breaking: climatology, interaction with low-frequency climate variability, and links to extreme weather events, pp. 69–78, Special Publications of the International Union of Geodesy and Geophysics, Cambridge University Press, https://doi.org/10.1017/CBO9781107775541.006, 2016.

Martius, O., Zenklusen, E., Schwierz, C., and Davies, H. C.: Episodes of Alpine heavy precipitation with an overlying elongated stratospheric intrusion: A climatology, International Journal of Climatology, 26, 1149–1164, https://doi.org/10.1002/joc.1295, 2006.

Martius, O., Schwierz, C., and Davies, H. C.: Tropopause-Level Waveguides, Journal of the Atmospheric Sciences, 67, 866–879, https://doi.org/10.1175/2009JAS2995.1, 2010.

Martius, O., Sodemann, H., Joos, H., Pfahl, S., Winschall, A., Croci-Maspoli, M., Graf, M., Madonna, E., Mueller, B., Schemm, S., Sedláček, J., Sprenger, M., and Wernli, H.: The role of upper-level dynamics and surface processes for the Pakistan flood of July 2010, Quarterly Journal of the Royal Meteorological Society, 139, 1780–1797, https://doi.org/10.1002/qj.2082, 2013.

Massacand, A. C., Wernli, H., and Davies, H. C.: Influence of upstream diabatic heating upon an Alpine event of heavy precipitation, Monthly Weather Review, 129, 2822–2828, https://doi.org/10.1175/1520-0493(2001)129<2822:IOUDHU>2.0.CO;2, 2001.

McIntyre, M. E. and Palmer, T.: Breaking planetary waves in the stratosphere, Nature, 305, 593, 1983.

Mo, K. C. and Livezey, R. E.: Tropical-Extratropical Geopotential Height Teleconnections during the Northern Hemisphere Winter, Monthly Weather Review, 114, 2488–2515, https://doi.org/10.1175/1520-0493(1986)114<2488:TEGHTD>2.0.CO;2, 1986.

Nakamura, H.: Midwinter Suppression of Baroclinic Wave Activity in the Pacific, Journal of the Atmospheric Sciences, 49, 1629–1642, https://doi.org/10.1175/1520-0469(1992)049<1629:MSOBWA>2.0.CO;2, 1992.

Nakamura, H. and Sampe, T.: Trapping of synoptic-scale disturbances into the North-Pacific subtropical jet core in midwinter, Geophysical Research Letters, 29, 8–1–8–4, https://doi.org/10.1029/2002GL015535, 2002.

Novak, L., Schneider, T., and Ait-Chaalal, F.: Midwinter suppression of storm tracks in an idealized zonally symmetric setting, Journal of the Atmospheric Sciences, 0, null, https://doi.org/10.1175/JAS-D-18-0353.1, 2020.

O'Gorman, P. A.: The Effective Static Stability Experienced by Eddies in a Moist Atmosphere, Journal of the Atmospheric Sciences, 68, 75–90, https://doi.org/10.1175/2010JAS3537.1, 2011.

Orlanski, I.: Bifurcation in Eddy Life Cycles: Implications for Storm Track Variability, Journal of the Atmospheric Sciences, 60, 993–1023, https://doi.org/10.1175/1520-0469(2003)60<993:BIELCI>2.0.CO;2, 2003.

Orlanski, I. and Chang, E. K. M.: Ageostrophic Geopotential Fluxes in Downstream and Upstream Development of Baroclinic Waves, Journal of the Atmospheric Sciences, 50, 212–225, https://doi.org/10.1175/1520-0469(1993)050<0212:AGFIDA>2.0.CO;2, 1993.

Papritz, L. and Schemm, S.: Development of an idealised downstream cyclone: Eulerian and Lagrangian perspective on the kinetic energy, Tellus A: Dynamic Meteorology and Oceanography, 65, 19 539, https://doi.org/10.3402/tellusa.v65i0.19539, 2013.

Penny, S., Roe, G. H., and Battisti, D. S.: The Source of the Midwinter Suppression in Storminess over the North Pacific, Journal of Climate, 23, 634–648, https://doi.org/10.1175/2009JCLI2904.1, 2010.

Penny, S. M., Roe, G. H., and Battisti, D. S.: Reply, Journal of Climate, 24, 5192–5194, https://doi.org/10.1175/2011JCLI4187.1, 2011.

Penny, S. M., Battisti, D. S., and Roe, G. H.: Examining Mechanisms of Variability within the Pacific Storm Track: Upstream Seeding and Jet-Core Strength, Journal of Climate, 26, 5242–5259, https://doi.org/10.1175/JCLI-D-12-00017.1, 2013.

Petterssen, S. and Smebye, S. J.: On the development of extratropical cyclones, Quarterly Journal of the Royal Meteorological Society, 97, 457–482, https://doi.org/10.1002/qj.49709741407, 1971.

Pfahl, S., Schwierz, C., Croci-Maspoli, M., Grams, C. M., and Wernli, H.: Importance of latent heat release in ascending air streams for atmospheric blocking, Nature Geoscience, 8, 610–614, https://doi.org/10.1038/NGEO2487, 2015.

Pomroy, H. R. and Thorpe, A. J.: The Evolution and Dynamical Role of Reduced Upper-Tropospheric Potential Vorticity in Intensive Observing Period One of FASTEX, Monthly Weather Review, 128, 1817–1834, https://doi.org/10.1175/1520-0493(2000)128<1817:TEADRO>2.0.CO;2, 2000.

Postel, G. A. and Hitchman, M. H.: A Climatology of Rossby Wave Breaking along the Subtropical Tropopause, Journal of the Atmospheric Sciences, 56, 359–373, https://doi.org/10.1175/1520-0469(1999)056<0359:ACORWB>2.0.CO;2, 1999.

Raveh-Rubin, S. and Flaounas, E.: A dynamical link between deep Atlantic extratropical cyclones and intense Mediterranean cyclones, Atmospheric Science Letters, 18, 215–221, https://doi.org/10.1002/asl.745, 2017.

Rivière, G. and Orlanski, I.: Characteristics of the Atlantic Storm-Track Eddy Activity and Its Relation with the North Atlantic Oscillation, Journal of the Atmospheric Sciences, 64, 241–266, https://doi.org/10.1175/JAS3850.1, 2007.

Rivière, G., Hua, B. L., and Klein, P.: Perturbation growth in terms of barotropic alignment properties, Quarterly Journal of the Royal Meteorological Society, 129, 2613–2635, https://doi.org/10.1256/qj.02.106, 2003.

Röthlisberger, M., Martius, O., and Wernli, H.: An algorithm for identifying the initiation of synoptic-scale Rossby waves on potential vorticity waveguides, Quarterly Journal of the Royal Meteorological Society, 142, 889–900, https://doi.org/10.1002/qj.2690, 2016.

Rüdisühli, S.: Attribution of Rain to Cyclones and Fronts Over Europe in a Kilometer-Scale Regional Climate Simulation, Ph.D. Thesis, ETH Zurich, p. 221pp, https://doi.org/10.3929/ethz-b-000351234, 2018.

Sanders, F.: Life History of Mobile Troughs in the Upper Westerlies, Monthly Weather Review, 116, 2629–2648, https://doi.org/10.1175/1520-0493(1988)116<2629:LHOMTI>2.0.CO;2, 1988.

Sanders, F. and Gyakum, J. R.: Synoptic-Dynamic Climatology of the "Bomb", Monthly Weather Review, 108, 1589–1606, https://doi.org/10.1175/1520-0493(1980)108<1589:SDCOT>2.0.CO;2, 1980.

Schemm, S.: Conveyor belts in idealized moist baroclinic wave life cycles, https://doi.org/10.3929/ethz-a-7632512, PhD Thesis, Dep. of Environmental Systems Science, ETH Zürich,190 pp., 2013.

Schemm, S. and Rivière, G.: On the Efficiency of Baroclinic Eddy Growth and How It Reduces the North Pacific Storm-Track Intensity in Midwinter, Journal of Climate, 32, 8373–8398, https://doi.org/10.1175/JCLI-D-19-0115.1, 2019.

Schemm, S. and Schneider, T.: Eddy Lifetime, Number, and Diffusivity and the Suppression of Eddy Kinetic Energy in Midwinter, Journal of Climate, 31, 5649–5665, https://doi.org/10.1175/JCLI-D-17-0644.1, 2018.

Schemm, S., Wernli, H., and Papritz, L.: Warm Conveyor Belts in Idealized Moist Baroclinic Wave Simulations, Journal of the Atmospheric Sciences, 70, 627–652, https://doi.org/10.1175/JAS-D-12-0147.1, 2013.

Schemm, S., Ciasto, L. M., Li, C., and Kvamstø, N. G.: Influence of Tropical Pacific Sea Surface Temperature on the Genesis of Gulf Stream Cyclones, Journal of the Atmospheric Sciences, 73, 4203–4214, https://doi.org/10.1175/JAS-D-16-0072.1, 2016.

Schemm, S., Rivière, G., Ciasto, L. M., and Li, C.: Extratropical Cyclogenesis Changes in Connection with Tropospheric ENSO Teleconnections to the North Atlantic: Role of Stationary and Transient Waves, Journal of the Atmospheric Sciences, 75, 3943–3964, https://doi.org/10.1175/JAS-D-17-0340.1, 2018.

Shapiro, M. A., Wernli, H., Bond, N. A., and Langland, R.: The influence of the 1997–99 El Niño Southern Oscillation on extratropical baroclinic life cycles over the eastern North Pacific, Quarterly Journal of the Royal Meteorological Society, 127, 331–342, https://doi.org/10.1002/qj.49712757205, 2001.

Simmons, A. J.: Numerical simulations of cyclone life cycles. Proceedings of an International Symposium on the Life Cycles of Extratropical Cyclones, vol. 1, Alma Mater Forlag, 1994.

Simmons, A. J. and Hoskins, B. J.: The Downstream and Upstream Development of Unstable Baroclinic Waves, Journal of the Atmospheric Sciences, 36, 1239–1254, https://doi.org/10.1175/1520-0469(1979)036<1239:TDAUDO>2.0.CO;2, 1979.

Sinclair, V. A., Rantanen, M., Haapanala, P., Räisänen, J., and Järvinen, H.: The characteristics and structure of extra-tropical cyclones in a warmer climate, Weather and Climate Dynamics, pp. 1–25, https://doi.org/10.5194/wcd-1-1-2020, 2020.

Spreitzer, E., Attinger, R., Boettcher, M., Forbes, R., Wernli, H., and Joos, H.: Modification of Potential Vorticity near the Tropopause by Nonconservative Processes in the ECMWF Model, Journal of the Atmospheric Sciences, 76, 1709–1726, https://doi.org/10.1175/JAS-D-18-0295.1, 2019.

Sprenger, M. and Wernli, H.: The LAGRANTO Lagrangian analysis tool – version 2.0, Geoscientific Model Development, 8, 2569–2586, https://doi.org/10.5194/gmd-8-2569-2015, https://www.geosci-model-dev.net/8/2569/2015/, 2015.

Sprenger, M., Fragkoulidis, G., Binder, H., Croci-Maspoli, M., Graf, P., Grams, C. M., Knippertz, P., Madonna, E., Schemm, S., Škerlak, B., and Wernli, H.: Global Climatologies of Eulerian and Lagrangian Flow Features based on ERA-Interim, Bulletin of the American Meteorological Society, 98, 1739–1748, https://doi.org/10.1175/BAMS-D-15-00299.1, 2017.

Stan, C., Straus, D. M., Frederiksen, J. S., Lin, H., Maloney, E. D., and Schumacher, C.: Review of Tropical-Extratropical Teleconnections on Intraseasonal Time Scales, Reviews of Geophysics, 55, 902–937, https://doi.org/10.1002/2016RG000538, 2017.

Starr, V. P.: An essay on the general circulation of the Earth's atmosphere, Journal of Meteorology, 5, 39–43, https://doi.org/10.1175/1520-0469(1948)005<0039:AEOTGC>2.0.CO;2, 1948.

Steinfeld, D. and Pfahl, S.: The role of latent heating in atmospheric blocking dynamics: a global climatology, Climate Dynamics, pp. 1–22, https://doi.org/10.1007/s00382-019-04919-6, 2019.

Stoelinga, M. T.: A Potential Vorticity-Based Study of the Role of Diabatic Heating and Friction in a Numerically Simulated Baroclinic Cyclone, Monthly Weather Review, 124, 849–874, https://doi.org/10.1175/1520-0493(1996)124<0849:APVBSO>2.0.CO;2, 1996.

Tamarin-Brodsky, T. and Hadas, O.: The Asymmetry of Vertical Velocity in Current and Future Climate, Geophysical Research Letters, 46, 374–382, https://doi.org/10.1029/2018GL080363, 2019.

Thorncroft, C. D., Hoskins, B. J., and McIntyre, M. E.: Two paradigms of baroclinic-wave life-cycle behaviour, Quarterly Journal of the Royal Meteorological Society, 119, 17–55, https://doi.org/10.1002/qj.49711950903, 1993.

Trenberth, K. E.: An Assessment of the Impact of Transient Eddies on the Zonal Flow during a Blocking Episode Using Localized Eliassen-Palm Flux Diagnostics, Journal of the Atmospheric Sciences, 43, 2070–2087, https://doi.org/10.1175/1520-0469(1986)043<2070:AAOTIO>2.0.CO;2, 1986.

Trigo, I. F., Bigg, G. R., and Davies, T. D.: Climatology of Cyclogenesis Mechanisms in the Mediterranean, Monthly Weather Review, 130, 549–569, https://doi.org/10.1175/1520-0493(2002)130<0549:COCMIT>2.0.CO;2, 2002.

Uccellini, L. W.: Processes contributing to the rapid development of extratropical cyclones, in: Extratropical cyclones, pp. 81–105, American Meteorological Society, Boston, MA, https://doi.org/10.1007/978-1-944970-33-8_6, 1990.

Wash, C. H., Peak, J. E., Calland, W. E., and Cook, W. A.: Diagnostic Study of Explosive Cyclogenesis during FGGE, Monthly Weather Review, 116, 431–451, https://doi.org/10.1175/1520-0493(1988)116<0431:DSOECD>2.0.CO;2, 1988.

Wernli, H.: A lagrangian-based analysis of extratropical cyclones. II: A detailed case-study, Quarterly Journal of the Royal Meteorological Society, 123, 1677–1706, https://doi.org/10.1002/qj.49712354211, 1997.

Wernli, H. and Davies, H. C.: A lagrangian-based analysis of extratropical cyclones. I: The method and some applications, Quarterly Journal of the Royal Meteorological Society, 123, 467–489, https://doi.org/10.1002/qj.49712353811, 1997.

Wernli, H. and Schwierz, C.: Surface Cyclones in the ERA-40 Dataset (1958–2001). Part I: Novel Identification Method and Global Climatology, Journal of the Atmospheric Sciences, 63, 2486–2507, https://doi.org/10.1175/JAS3766.1, 2006.

Wernli, H. and Sprenger, M.: Identification and ERA-15 Climatology of Potential Vorticity Streamers and Cutoffs near the Extratropical Tropopause, Journal of the Atmospheric Sciences, 64, 1569–1586, https://doi.org/10.1175/JAS3912.1, 2007.

Wernli, H., Dirren, S., Liniger, M. A., and Zillig, M.: Dynamical aspects of the life cycle of the winter storm 'Lothar' (24–26 December 1999), Quarterly Journal of the Royal Meteorological Society, 128, 405–429, https://doi.org/10.1256/003590002321042036, 2002.

Yeh, S.-W., Cai, W., Min, S.-K., McPhaden, M. J., Dommenget, D., Dewitte, B., Collins, M., Ashok, K., An, S.-I., Yim, B.-Y., and Kug, J.-S.: ENSO Atmospheric Teleconnections and Their Response to Greenhouse Gas Forcing, Reviews of Geophysics, 56, 185–206, 2018.

740 Yuval, J., Afargan, H., and Kaspi, Y.: The Relation Between the Seasonal Changes in Jet Characteristics and the Pacific Midwinter Minimum in Eddy Activity, Geophysical Research Letters, 45, 9995–10 002, https://doi.org/10.1029/2018GL078678, 2018.

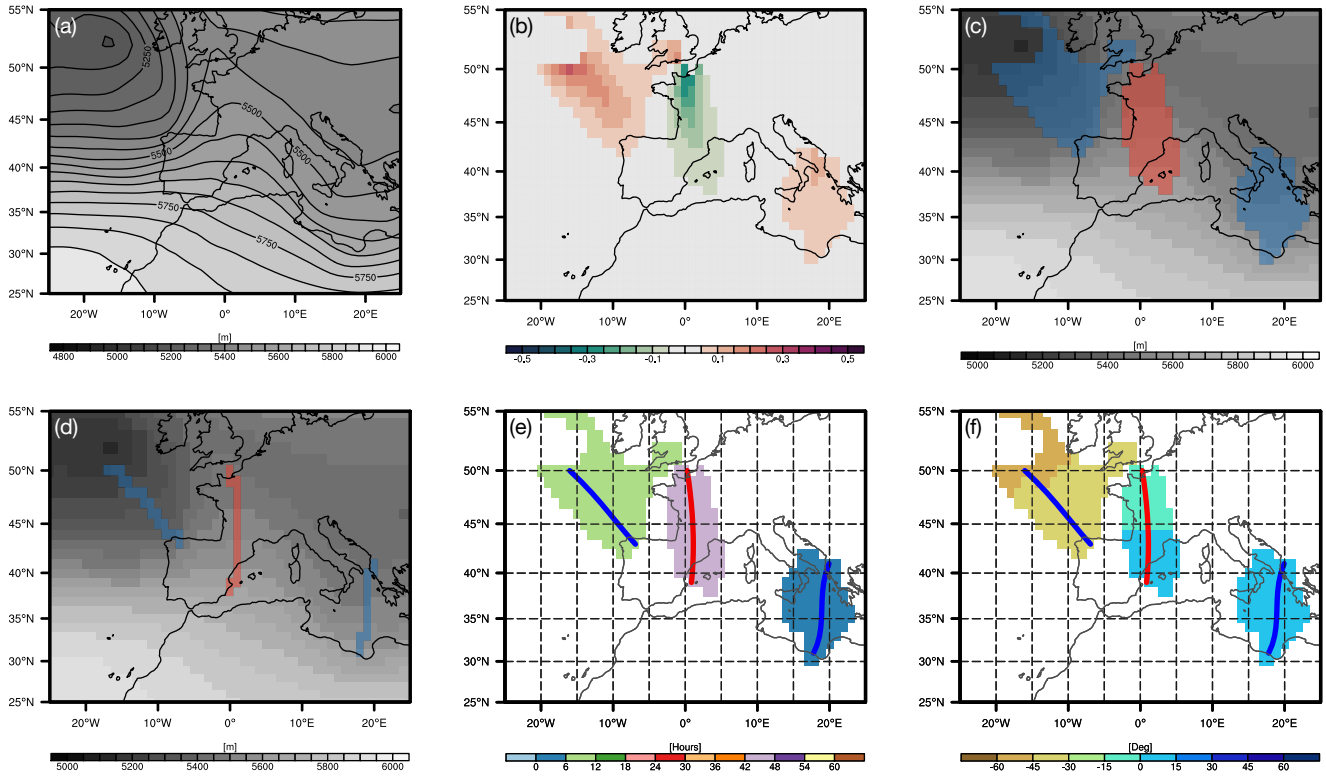

Figure 1. (a) ~~500-hPa~~ 500 hPa geopotential height (m) at 12 UTC on 12 January 2010~~,~~; (b) curvature of the geopotential isolines (units: degrees per kilometer) on the $1^\circ \times 1^\circ$ input grid at every grid point where the curvature is larger than 0.05 degrees per km; (c) 2D trough (blue) and ridge (red) masks and geopotential height (gray shading) at every grid point; (d) ~~Corresponding~~ corresponding trough (blue) and ridge (red) axes; (e) ~~Cubic-spline~~ cubic-spline interpolated trough and ridge axes and age (color; in hours) of the trough and ridge features; (f) ~~Horizontal~~ horizontal orientation of the trough and ridge object (in degrees; angle relative to a north-south meridian and estimated from the corresponding axis).

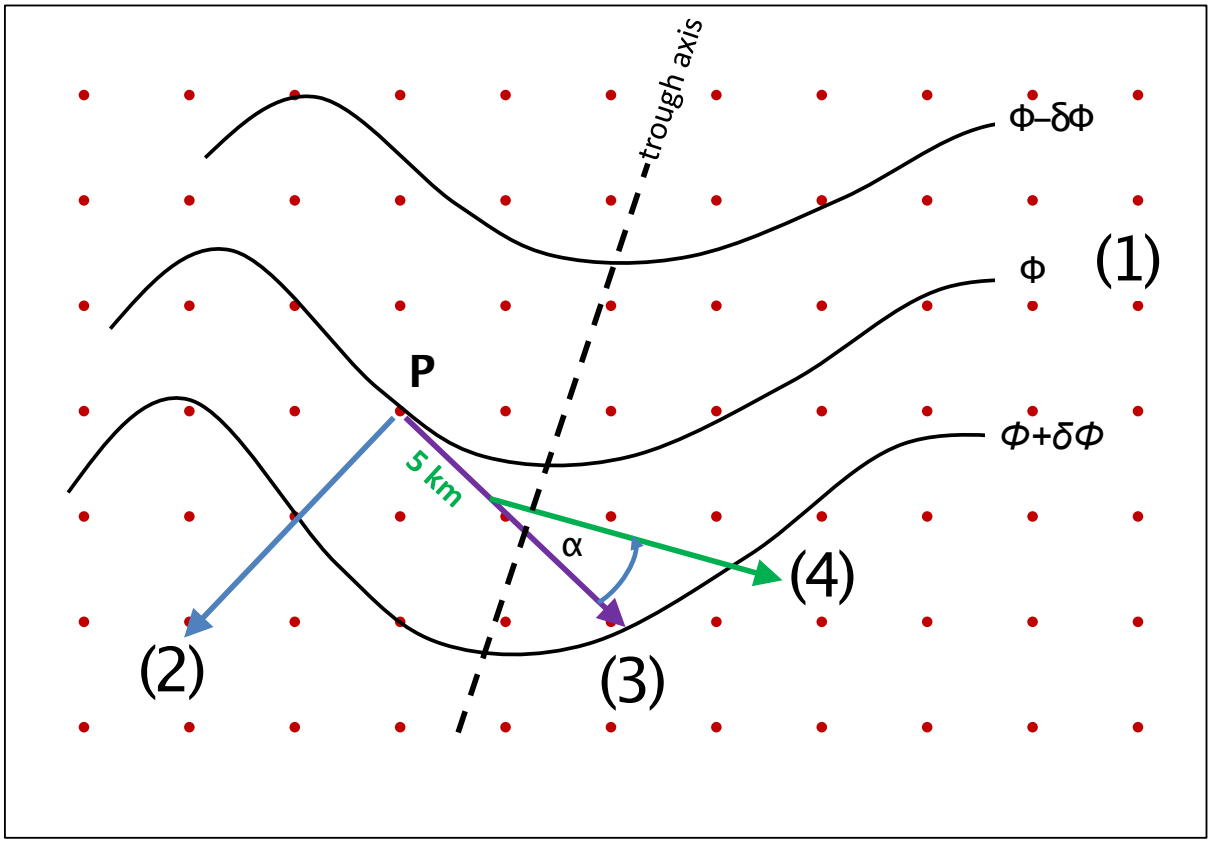

Figure 2. ~~500-hPa trough~~ Schematic showing the different steps in determining the local curvature of the geopotential height isolines. The steps are: (~~blue~~1) ~~and ridge~~ geopotential height isolines (~~red~~black contours) ~~axes~~ at every grid values (~~a~~red points)~~06 UTC and~~ ; (~~b~~2) ~~12 UTC on 12 January 2010, quasi-geostrophic omega~~ local gradient vector (~~from 0.1 to 1 in steps~~ blue) of ~~0.1 m s^{-1}~~the geopotential height at a specific grid point P; ~~positive values~~ (3) 90-degree rotated vector (purple) to get a tangent vector parallel to the geopotential height isolines; (4) a forward step by 5 km in ~~yellow indicate descent~~ the direction of the geopotential-parallel vector and ~~negative values in~~ a new parallel vector (green~~indicate ascent~~) interpolated to the new position; (5) calculating the angle α between the vectors (3) and ~~geopotential height~~ (~~m; gray shading~~4). For further details, see text.

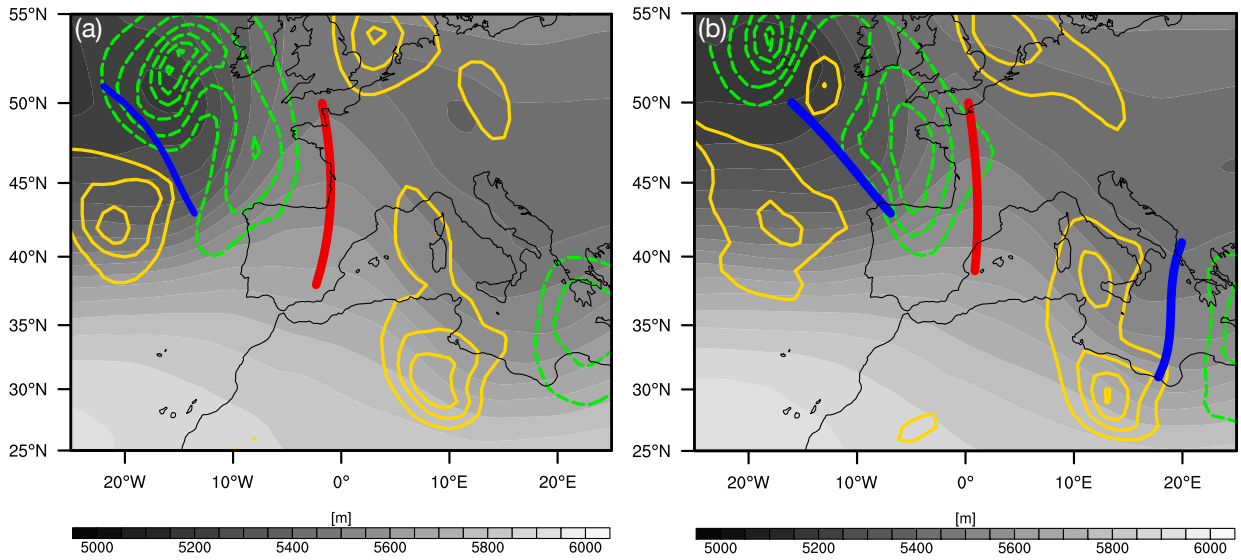

Figure 3. 500 hPa trough (blue) and ridge (red) axes at (a) 06 UTC and (b) 12 UTC on 12 January 2010, quasi-geostrophic omega (from 0.1 to 1 in steps of 0.1 m s^{-1}; positive values in yellow indicate descent and negative values in green indicate ascent) and geopotential height (m; gray shading).

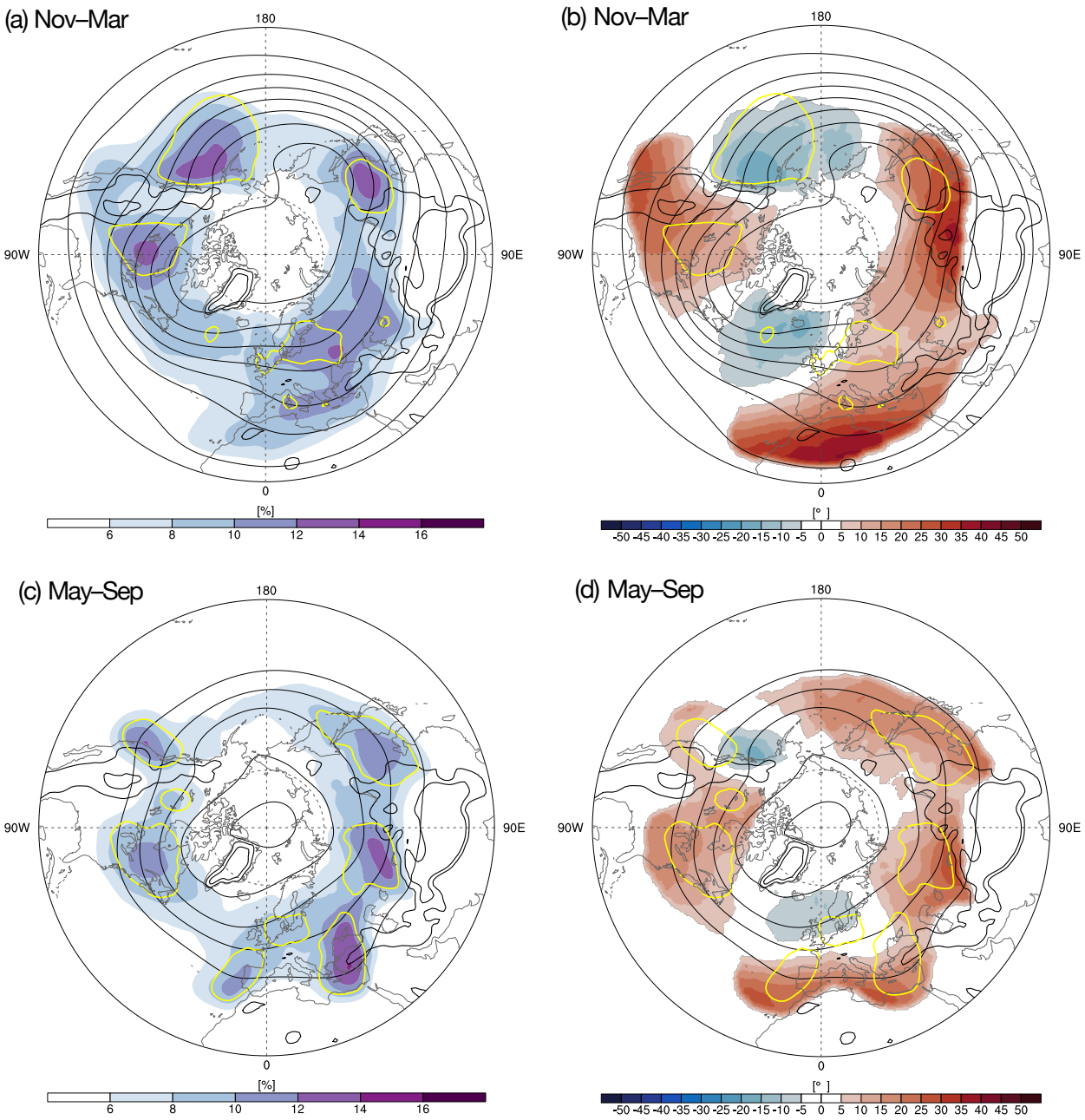

Figure 4. Left column: Seasonal climatologies of the trough detection frequencies (color shading; units: %) for the cold (a; Nov–Mar) and warm (c; May–Sep) seasons. Additional contours show selected frequencies of troughs with an age between 0 and 24 hours (yellow). Right column: Seasonal climatologies of the corresponding horizontal trough orientation on the ~~500 hPa~~ 500 hPa level (color shading; units: degrees) for the cold (b; Nov–Mar) and warm (d; May–Sep) seasons~~.~~. Positive values indicate anticyclonically oriented troughs. Additionally, the yellow 0–24-hour age contour, similar to that in (a, c), is shown for reference. The 1,500-m height contour (black) is shown in all the panels.

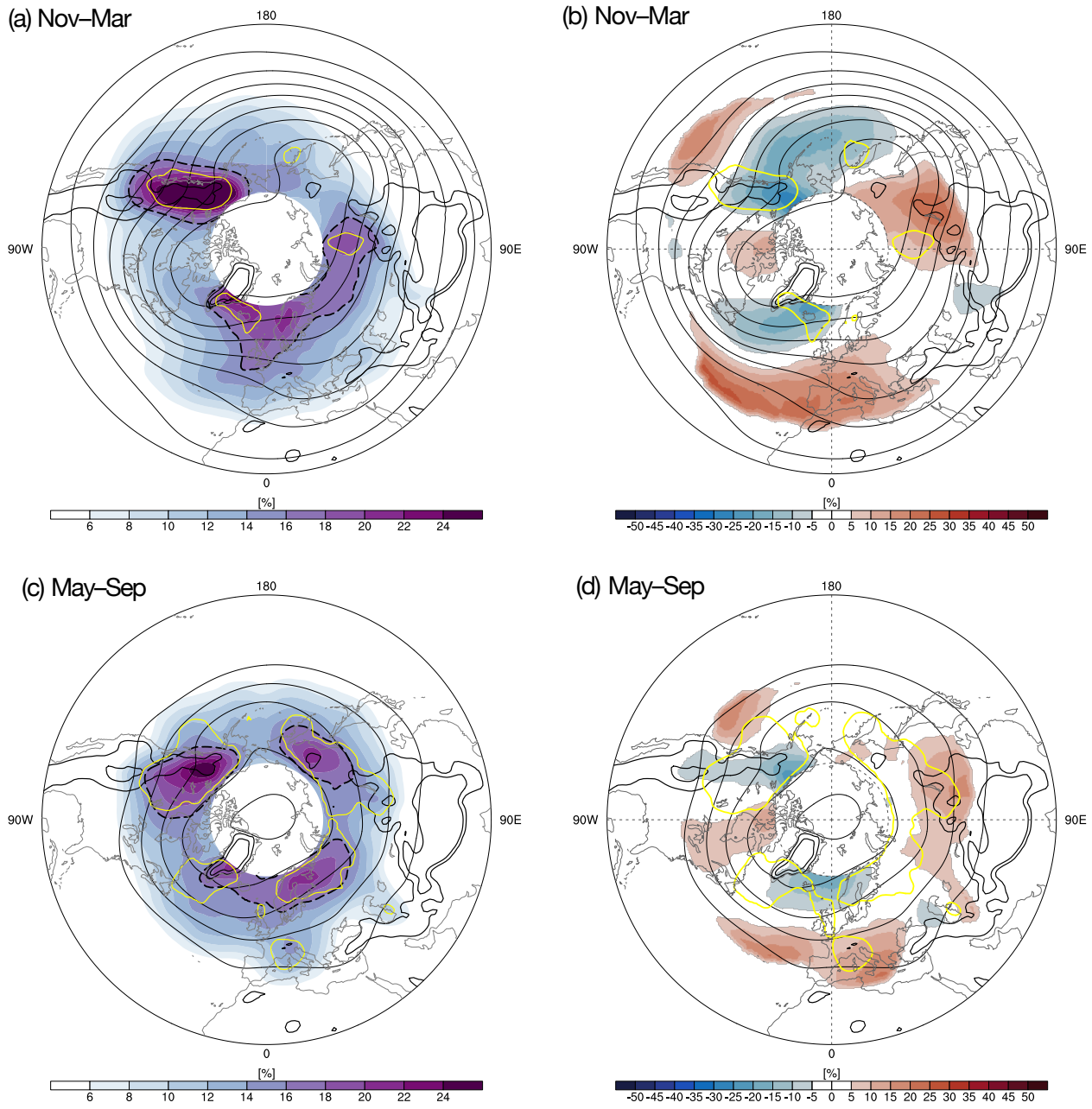

Figure 5. Similar to Fig. 4 but for ridges. The dashed contour indicates the region where the ridge frequency is above the maximum global trough detection frequency ($\approx 16\,\%$).

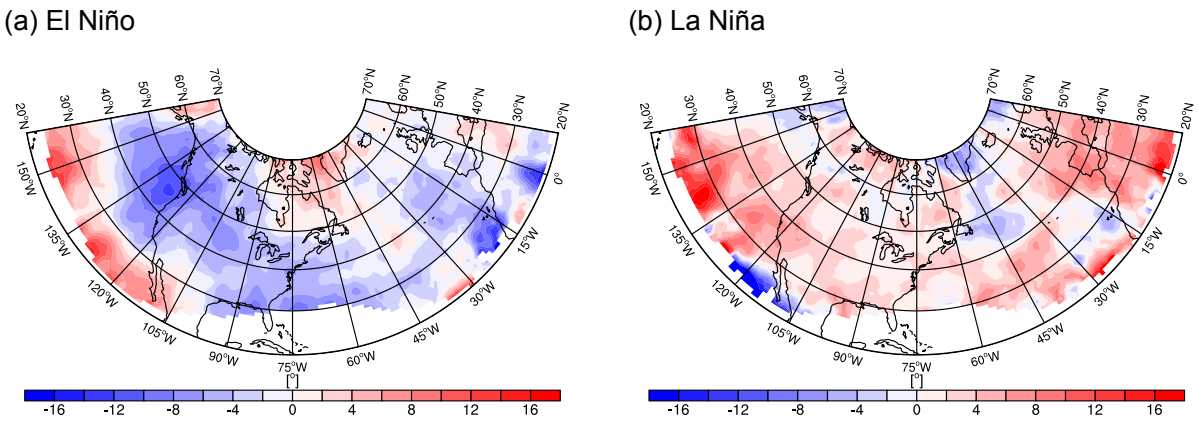

Figure 6. Averaged orientation anomalies (units: degrees) of ~~500 hPa~~ 500 hPa troughs and ridges during (a) El Niño- and (b) La Niña-affected winter seasons. (Positive) Negative anomalies indicate more (anti)cyclonically oriented troughs and ridges compared to the seasonal climatology. Regions where the detection frequency is below 2 % are excluded.

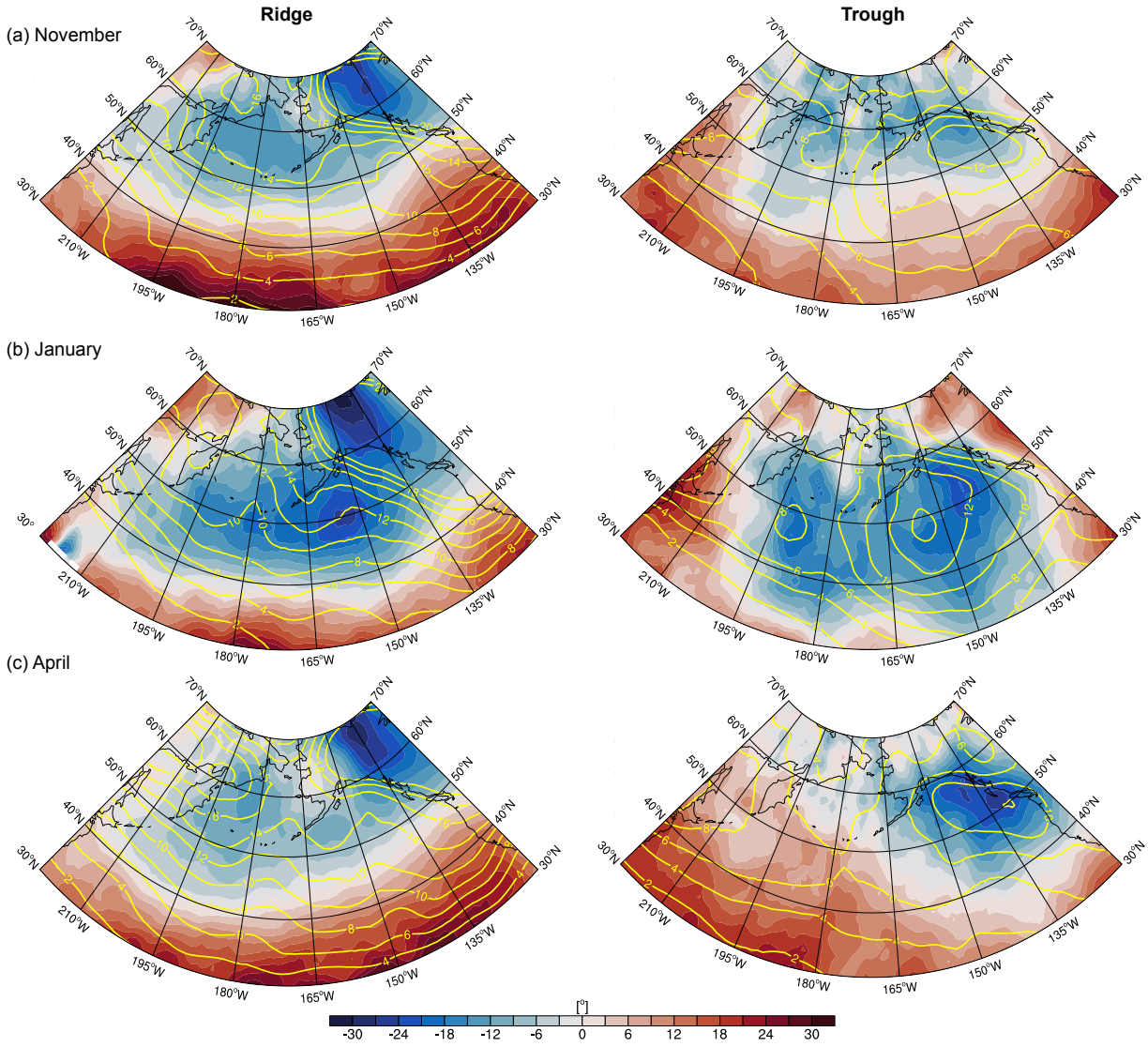

Figure 7. Monthly mean orientation (color shading; degrees) ~~of 500-hPa troughs~~ and frequency (yellow contours, from 2 to 14 % in steps of 2 %) of 500 hPa ridges and troughs during (a) October, (b) January and (c) April over the North Pacific.

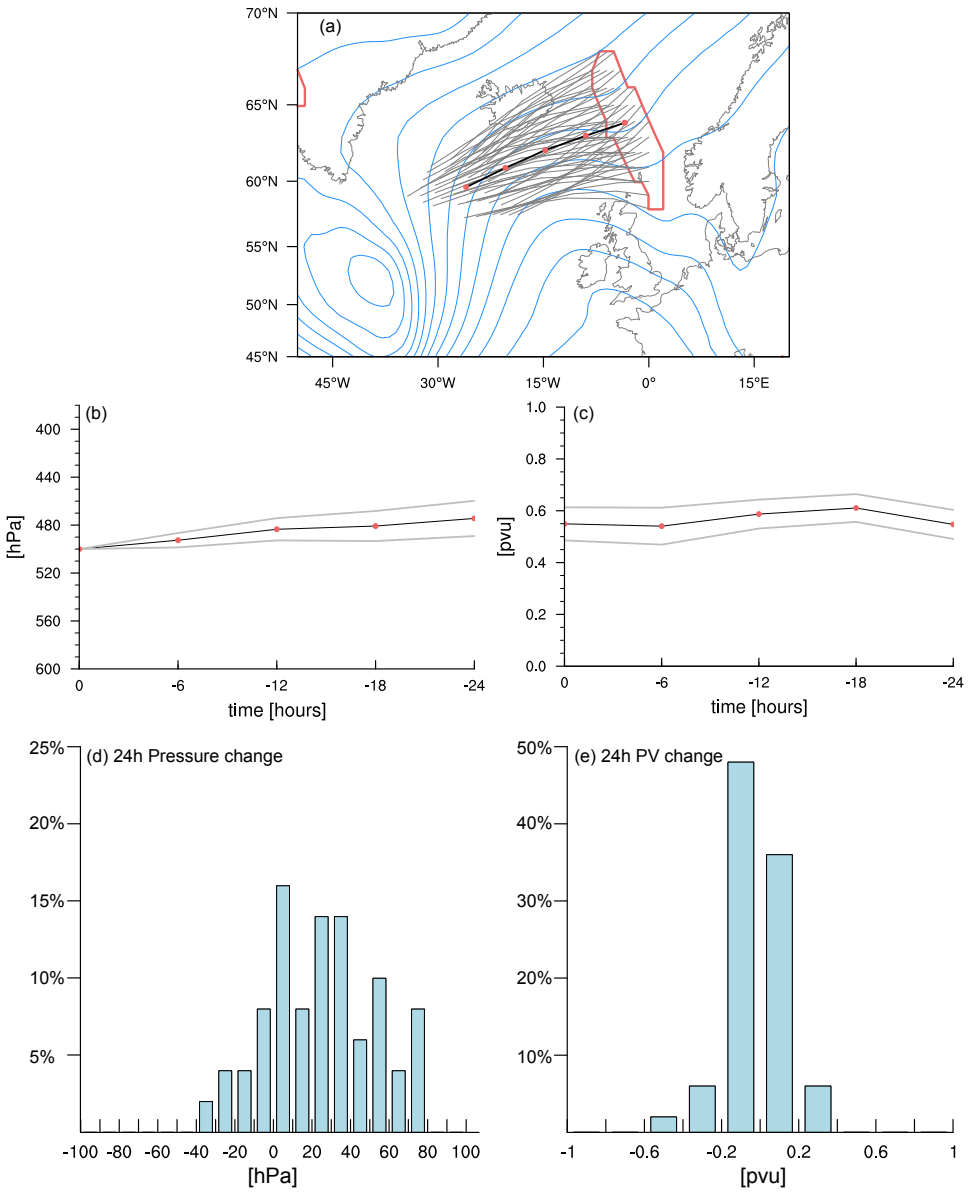

Figure 8. (a) Twenty-four-hour backward trajectories (gray lines) released on 18:00 UTC 18 January 2010 from a trough feature (red contours) at 500 hPa. The black contour indicates the average over all the trajectories. Red dots indicate 6-hourly time steps. Geopotential heights are shown as blue contours (5000 to 5600 m in steps of 50 m). (b) Mean pressure evolution (black; hPa) along the backward trajectories shown in (a). The standard deviation across the sample is indicated by thin gray lines. Red dots denote 6-hour steps. (c) Similar to (b) but for the potential vorticity (pvu). (d,e) Histograms of the 24-hour changes in pressure (hPa day^{-1}) and potential vorticity (pvu day^{-1})

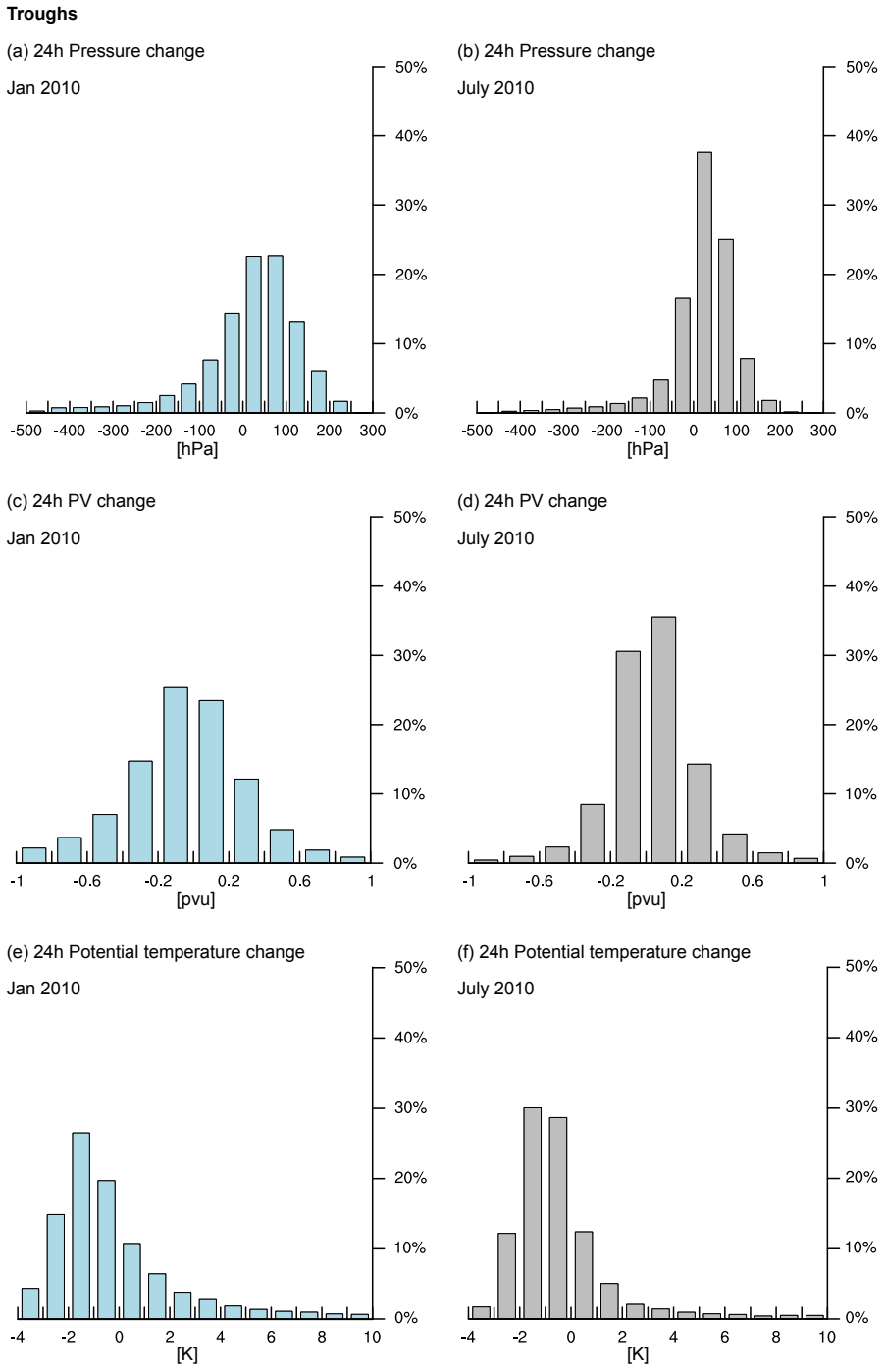

Figure 9. Histograms of the change (a, b) in pressure (hPa day^{-1}), (c, d) the potential vorticity (pvu day^{-1}) and (e, f) potential temperature (K day^{-1}) along the ~~flow of~~ air parcel trajectories released from all troughs detected at the ~~500 hPa~~ 500 hPa level during (a, c) January and (b, d) July 2010.

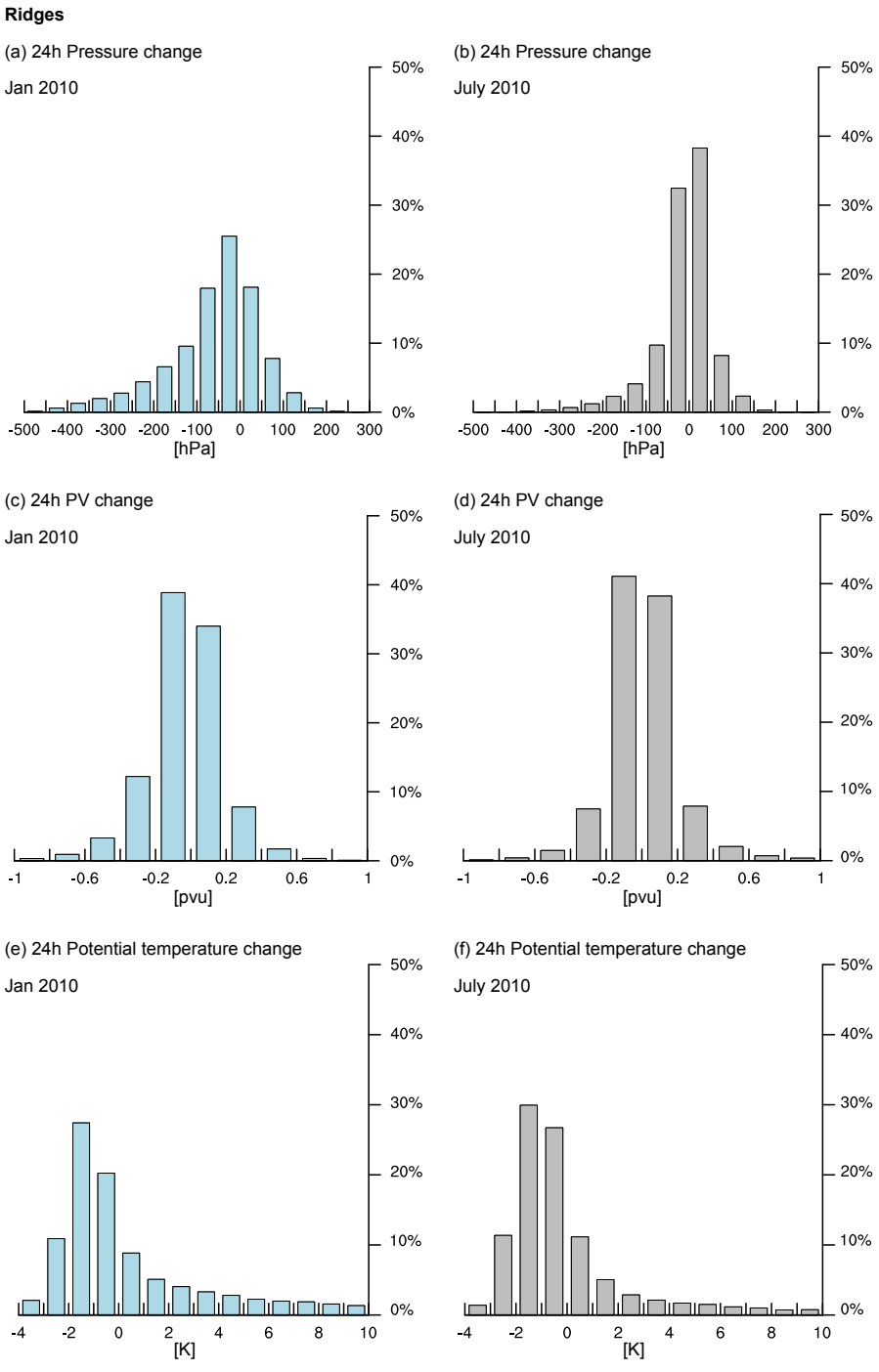

Figure 10. Similar to Fig. 9 but for ~~500 hPa~~ 500 hPa ridges.